frontiers in Marine Science

ORIGINAL RESEARCH
published: 07 January 2022
doi: 10.3389/fmars.2021.782734

Trace Metal Dynamics in Shallow Hydrothermal Plumes at the Kermadec Arc

Charlotte Kleint[1,2], Rebecca Zitoun[3,4,5], René Neuholz[6,7], Maren Walter[2,8], Bernhard Schnetger[6], Lukas Klose[1,2], Stephen M. Chiswell[9], Rob Middag[5], Patrick Laan[5], Sylvia G. Sander[3,4] and Andrea Koschinsky[1,2]*

[1] Department of Physics and Earth Sciences, Jacobs University Bremen, Bremen, Germany, [2] Center for Marine Environmental Sciences (MARUM), University of Bremen, Bremen, Germany, [3] Marine Mineral Resources, Dynamics of the Ocean Floor Division, GEOMAR Helmholtz Center for Ocean Research Kiel, Kiel, Germany, [4] Department of Chemistry, University of Otago, Dunedin, New Zealand, [5] Royal Netherlands Institute for Sea Research (NIOZ), Texel, Netherlands, [6] Institute for Chemistry and Biology of the Marine Environment, University of Oldenburg, Oldenburg, Germany, [7] Fraunhofer Institute for Manufacturing Technology and Advanced Materials (FHG), Bremen, Germany, [8] Institute of Environmental Physics, University of Bremen, Bremen, Germany, [9] National Institute of Water and Atmospheric Research (NIWA), Wellington, New Zealand

OPEN ACCESS

Edited by:
Johan Schijf,
University of Maryland Center for Environmental Science (UMCES), United States

Reviewed by:
Guy Evans,
University of Minnesota Twin Cities, United States
Torben Stichel,
Alfred Wegener Institute Helmholtz Centre for Polar and Marine Research (AWI), Germany

***Correspondence:**
Charlotte Kleint
C.Kleint@jacobs-university.de

Specialty section:
This article was submitted to Marine Biogeochemistry, a section of the journal Frontiers in Marine Science

Received: 24 September 2021
Accepted: 08 December 2021
Published: 07 January 2022

Citation:
Kleint C, Zitoun R, Neuholz R, Walter M, Schnetger B, Klose L, Chiswell SM, Middag R, Laan P, Sander SG and Koschinsky A (2022) Trace Metal Dynamics in Shallow Hydrothermal Plumes at the Kermadec Arc. Front. Mar. Sci. 8:782734. doi: 10.3389/fmars.2021.782734

Hydrothermal vents are a source of many trace metals to the oceans. Compared to mid-ocean ridges, hydrothermal vent systems at arcs occur in shallower water depth and are much more diverse in fluid composition, resulting in highly variable water column trace metal concentrations. However, only few studies have focused on trace metal dynamics in hydrothermal plumes at volcanic arcs. During R/V Sonne cruise SO253 in 2016/2017, hydrothermal plumes from two hydrothermally active submarine volcanoes along the Kermadec arc in the Southwest Pacific Ocean were sampled: (1) Macauley, a magmatic dominated vent site located in water depths between 300 and 680 m, and (2) Brothers, located between 1,200 and 1,600 m water depth, where hydrothermalism influenced by water rock interactions and magmatically influenced vent sites occur near each other. Surface currents estimated from satellite-altimeter derived currents and direct measurements at the sites using lowered acoustic Doppler current profilers indicate the oceanic regime is dominated by mesoscale eddies. At both volcanoes, results indicated strong plumes of dissolved trace metals, notably Mn, Fe, Co, Ni, Cu, Zn, Cd, La, and Pb, some of which are essential micronutrients. Dissolved metal concentrations commonly decreased with distance from the vents, as to be expected, however, certain element/Fe ratios increased, suggesting a higher solubility of these elements and/or their stronger stabilization (e.g., for Zn compared to Fe). Our data indicate that at the magmatically influenced Macauley and Brothers cone sites, the transport of trace metals is strongly controlled by sulfide nanoparticles, while at the Brothers NW caldera wall site iron oxyhydroxides seem to dominate the trace metal transport over sulfides. Solution stabilization of trace metals by organic complexation appears to compete with

particle adsorption processes. As well as extending the generally sparse data set for hydrothermal plumes at volcanic arc systems, our study presents the first data on several dissolved trace metals in the Macauley system, and extends the existing plume dataset of Brothers volcano. Our data further indicate that chemical signatures and processes at arc volcanoes are highly diverse, even on small scales.

Keywords: trace metals, hydrothermal plumes, South Pacific Ocean, plume dispersion, arc hydrothermalism, Macauley volcano, Brothers volcano

INTRODUCTION

Many trace metals, including manganese (Mn), iron (Fe), copper (Cu), nickel (Ni), zinc (Zn), cobalt (Co), cadmium (Cd) and the light rare earth elements, e.g., lanthanum (La) are essential micronutrients for most marine organisms. Some of these metals, particularly Fe, are depleted in large areas of the surface oceans, limiting ocean primary productivity (Sunda, 1988; Whitfield, 2001; Morel et al., 2003; Hassler et al., 2012; Butler et al., 2013). Some elements, such as lead (Pb) but also La, Cu, Zn, and Cd can, however, also be inhibitory or toxic to marine organisms at concentrations already slightly above their essential threshold (Sunda, 1988; Jin et al., 2009; Echeveste et al., 2012). Hydrothermal vents release large amounts of this suite of elements into the ocean, and several studies suggest that the role of hydrothermal trace metal input on the biogeochemical cycle of key micronutrients, especially Fe, in the ocean is significant (Boyd and Ellwood, 2010; Sander and Koschinsky, 2011; Fitzsimmons et al., 2014; Tagliabue, 2014; German et al., 2016; Schlitzer et al., 2018; Ardyna et al., 2019).

The distribution, concentration, and speciation of hydrothermally derived metals in the water column are inherently linked to buoyancy-driven vertical mixing and lateral spreading of the plume, two processes that are affected by chemical processes (German et al., 1991; Rudnicki and Elderfield, 1993; Baker et al., 1995). For example, oxidation of dissolved Fe^{2+} during mixing of the plume with ambient seawater will lead to the formation of particles (e.g., Fe oxyhydroxides), that will sink and settle to the seafloor where they will deposit as metalliferous sediments (Millero et al., 1987; Santana-Casiano et al., 2006). Hydrothermally derived metals can, however, also be stabilized in their dissolved form (operationally defined as the fraction left after 0.2 μm filtration) either by inorganic complexation, e.g., as sulfide complexes or nanoparticles (Yücel et al., 2011; Gartman et al., 2014; Lough et al., 2019b) or by organic complexation, e.g., by colloidal bulk organic matter, or by smaller, metal chelating molecules—so called ligands (Bennett et al., 2008; Toner et al., 2009; Sander and Koschinsky, 2011; Kleint et al., 2016). A recent study of hydrothermal plumes on the northern Mid-Atlantic Ridge showed that organic ligands and colloidal-size particles decrease the oxidation rate of Fe^{2+} in the plume (González-Santana et al., 2021), preventing Fe from oxidation, sorption, and settling. Such processes might also lead to a decreased rate in sorption and settling of other hydrothermally derived trace metals, thereby allowing them to be transported potentially thousands of kilometers from their original source into the distal ocean. Recent studies have demonstrated long-range transport of hydrothermally derived dissolved Fe and Mn from the East Pacific Rise as far as 4000 km, with postulated wide ranging effects on global Fe and Mn cycles (Resing et al., 2015; Fitzsimmons et al., 2017).

So far, most studies have focused on the transport and biogeochemical behavior of hydrothermally derived Fe and Mn (Hawkes et al., 2013; Hatta et al., 2015; Resing et al., 2015; Fitzsimmons et al., 2017; Lough et al., 2019b; González-Santana et al., 2020, 2021; Jenkins et al., 2020; Roshan et al., 2020). Other metals have received far less attention, and only a few studies have published data related to hydrothermal Cu (Sarradin et al., 2009; Cotte et al., 2018; Ruacho et al., 2020), Zn (Conway and John, 2014; Roshan et al., 2016), Co (Hawco et al., 2016), Ni (Stüben et al., 1992), Cd (James and Elderfield, 1996), Pb (Noble et al., 2015), and La (Stichel et al., 2018), or a combination of the previously mentioned elements (Haalboom et al., 2020). Therefore, little is known about the concentrations, distribution, and dispersal of the range of these elements within a single plume system. In order to get a complete understanding of the importance of arc systems for the marine trace metal and nutrient cycle, it is important to study metal micronutrients as well as macronutrients at the same time.

Macronutrients, such as phosphate (PO_4), nitrate + nitrite (NO_x), and silicate (SiO_2) are also very important in ocean biogeochemical processes as they are essential for the growth of marine phytoplankton in seawater and can thereby limit primary productivity (Wheat et al., 1996; Feely et al., 1998; Bristow et al., 2017). It is known that hydrothermal processes play an important role in the global cycles (e.g., dissolved PO_4 is removed from the plumes and the water column by coprecipitation onto Fe-oxyhydroxides, Wheat et al., 1996).

So far, most plume studies have been carried out at mid-ocean ridge systems, and only a few publications report on trace metals (namely Fe and Mn) in plumes of volcanic arc systems (e.g., Massoth et al., 2003; Resing et al., 2009). Due to the shallower water depth of volcanic arcs compared to mid-ocean ridges, their hydrothermal plumes may reach surface waters and thus directly supply essential nutrients into the photic zone, making these systems invaluable to study. Furthermore, volcanic-hosted vent systems can show a very large diversity in fluid composition, reflecting different magmatic and water-rock interaction sources. Especially the dynamics, speciation, and initial fluid concentrations of Fe and H_2S are important, as both species are extremely sensitive to oxidation in the early plume. Thus, Fe and H_2S dominate fluid chemistry in most vent systems and are the key factors in affecting the speciation and

concentration of other elements, such as Zn, Cu, Co, Pb, and Cd (Mottl and McConachy, 1990; Findlay et al., 2019).

To better understand the importance of these systems to the overall nutrient cycle in shallow volcanic arc system plumes, we sampled hydrothermal plumes at two submarine volcanoes at the Kermadec arc in the Southwest Pacific. The Kermadec arc, a 2500 km intraoceanic arc, is located northeast of New Zealand, where the Pacific plate is subducted beneath the Australian plate (de Ronde et al., 2003). Samples were taken at Macauley and Brothers volcanoes (**Figure 1**) in December 2016 and January 2017, respectively. Trace metal dynamics (Mn, Fe, Co, Ni, Cu, Zn, Cd, La, and Pb) in hydrothermal plumes were evaluated using hydrothermal tracers, including turbidity anomalies, and δ^3He and Ra isotopes (Neuholz et al., 2020b).

Apart from one other study by de Ronde et al. (2007), who determined dissolved Fe and Mn, the plumes of Macauley have not been geochemically analyzed for dissolved trace metals. Brothers volcano is one of the most extensively studied submarine arc volcanoes (Kleint et al., 2019; de Ronde et al., 2012; and references therein), with considerable oceanographic mapping and monitoring (Baker et al., 2012; Walker et al., 2018). However, to the best of our knowledge, no detailed information on the Brothers hydrothermal plume chemistry exists, apart from a few observations of dissolved Fe, Mn, gases, and particulates (de Ronde et al., 2005), and one study also from this SO253 cruise (Neuholz et al., 2020a). Therefore, to our knowledge, this study presents the first data on several dissolved trace metals, other than Fe and Mn, in hydrothermal plumes of the Macauley system and over the Brothers caldera.

MATERIALS AND METHODS

Working Area and Sample Collection

Hydrothermal plume samples were collected during R/V Sonne cruise SO253 between December 2016 and January 2017 at the two different active caldera volcanoes, Macauley and Brothers (**Figure 1**). Data from this cruise showed that the fluids

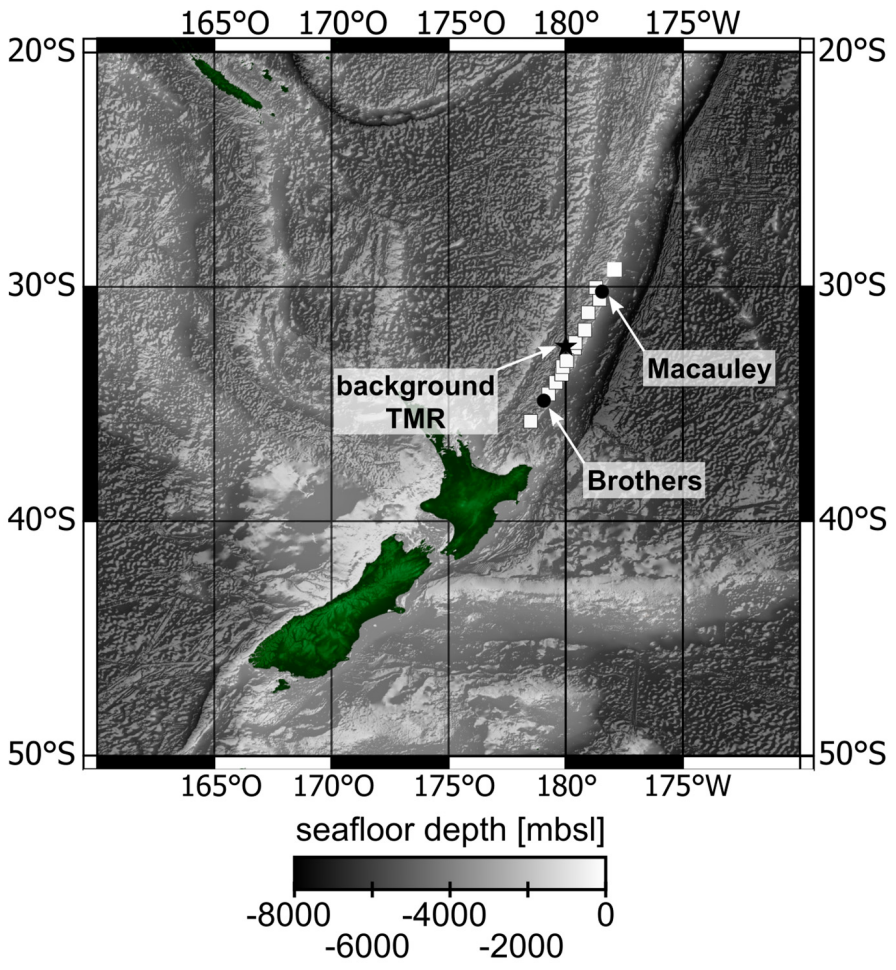

FIGURE 1 | Map of the southern Kermadec arc, showing the locations of the two sampled working areas, Macauley volcano (sampled between December 26th and 29th 2016) and Brothers volcano (sampled between January 7th and 17th 2017), as well as other active hydrothermal vent sites (white squares, de Ronde et al., 2007). The background station (station 28 from GP13) was sampled with a TMR (trace metal-clean rosette) (GEBCO Bathymetric Compilation Group, 2020).

between 330 and 680 m at the magmatically influenced site at Macauley are metal and sulfide rich acid-sulfate type fluids with maximum temperatures of 112°C and minimum pH values of 1.2 (Kleint et al., 2019), while the Brothers volcano is dominated by two different vent systems. One vent system is located at the northwest caldera wall, where water-rock interactions result in high-temperature black smoker fluids (max. measured temperature: 311°C; minimum pH: 3.1) at ∼1,600 m (Kleint et al., 2019). The other system is located at the southeast cone site, where magmatically influenced clear fluids are being expelled at maximum temperatures of 115°C and minimum pH values of 2.1 between ∼1,200 and 1,300 m (de Ronde et al., 2011; Kleint et al., 2019).

The ocean circulation around the Kermadec arc is generally weak, largely because the arc is close to the center of the South Pacific Ocean subtropical gyre (Morris et al., 1996; Sutton et al., 2012). To the south of the region, the East Auckland Current runs southwest along the east coast of the North Island of New Zealand and in the mean the surface currents show two semi-permanent eddies, the North Cape Eddy, situated north of North Cape, and the East Cape Eddy situated north of East Cape (Roemmich and Sutton, 1998; Chiswell et al., 2015). These eddies are known to fluctuate in intensity and location (Chiswell, 2005), and thus because of the generally weak circulation, lateral spreading of the hydrothermal plumes will be determined by the mesoscale eddy field.

A standard shipboard CTD carousel water sampler (SBE 9plus with SBE 32, hereafter "CTD") equipped with two Seapoint Turbidity Meters (5x gain) deployed on a steel hydrowire, and a trace metal-clean rosette (hereafter called TMR) equipped with 12 acid cleaned Teflon-coated polyvinylchloride (PVC) 5 L GO-FLO bottles (General Oceanics Inc.) deployed on a Dyneema rope, were used to sample the hydrothermal plumes above and in the near-field of the volcanoes (**Figure 2**). Locations closer than 5 km to the known vent sites were sampled with the CTD water sampler, to avoid contamination of the TMR with high metal concentrations. The TMR was only used further than 5 km from active vents (where there were presumably lower metal concentrations). One TMR (080), which was initially planned as the background TMR for this study was found to be influenced by hydrothermal signals, evident by elevated trace metal concentrations (data not shown). We therefore used background trace metal concentrations of Station 28 over the Kermadec arc (180°E, 32.5°S, **Figure 1** and **Supplementary Table 2**) from the GEOTRACES Australian/New Zealand transect GP13, taken in 2011 and reported in the GEOTRACES intermediate data product 2017 (Schlitzer et al., 2018). Unfortunately, data for Co and La were not generated during the GP13 transect.

At Macauley, plume surveys included three vertical CTD casts and two tow-yos (during the latter, the CTD is towed behind the moving ship, while being raised and lowered through the water column). The three vertical casts were made directly at the cone where active venting is present at ∼330 m (CTD 006), ∼0.4 km west of the cone (CTD 019) and ∼1.25 km west of the cone (CTD 012) where another vent system is present at ∼680 m (Kleint et al., 2019). One tow-yo (CTD-T 004) was carried out in an east-southwestern direction directly above the three vertical CTD casts, while the other tow-yo (CTD-T 010) was carried out in southeast-northwest direction (**Supplementary Table 1** and **Figure 2**).

At Brothers, six vertical CTD and TMR casts were carried out, three of them inside the caldera (CTD 053, CTD 054 and CTD 058), and three outside of the caldera (TMR 060, TMR 070 and

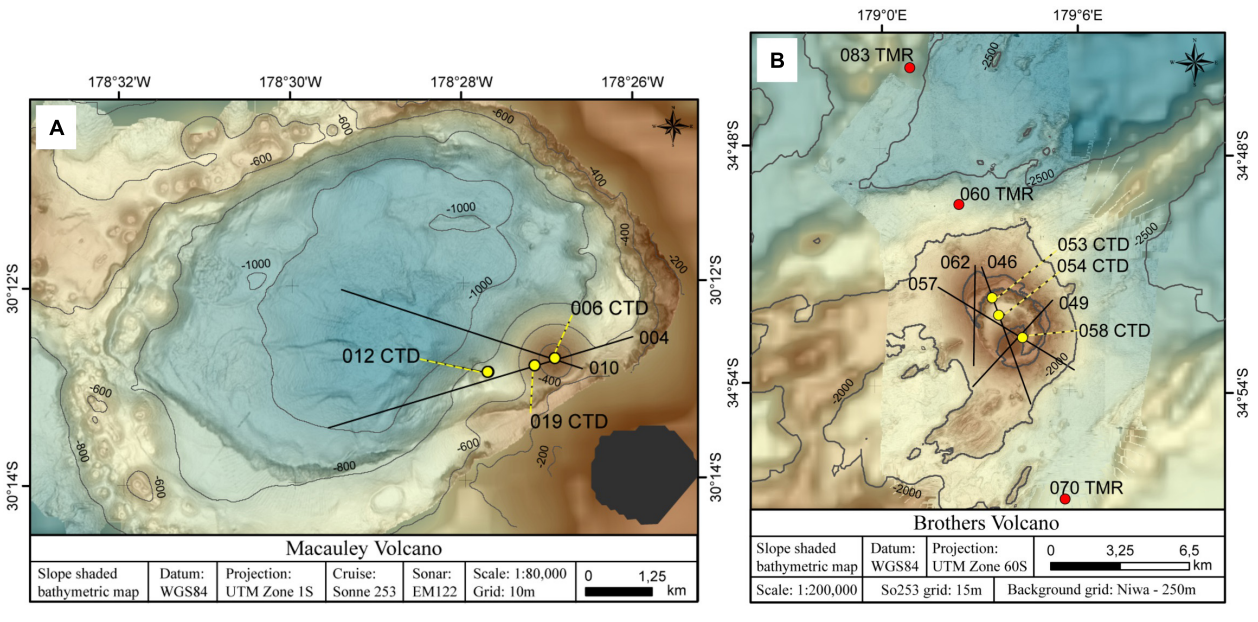

FIGURE 2 | Bathymetric map of the two active submarine volcanoes Macauley **(A)** and Brothers **(B)** including the sampled vertical CTDs (yellow dots), TMRs (red dots), and conducted tow-yos (black lines)© Dr. Janis Thal, University of Bremen.

TMR 083; **Supplementary Table 1** and **Figure 2**). CTDs 053 and 054 were deployed close to the vents at the NW caldera wall, while CTD 058 was taken closer to the cone site. TMR 070 was taken 10 km to the southeast of the caldera, while TMR 060 and TMR 083 were taken 6 and 12 km to the northwest, respectively. All vertical CTDs were taken along a southeast-northwest-transect, following the main current direction. Four tow-yos (CTD-T 046, CTD-T 049, CTD-T 057, CTD-T 062) were carried out inside and outside of the caldera (**Supplementary Table 1** and **Figure 2**).

Methods and Analysis

Dissolved Trace Metals

For trace metal analyses at the CTD stations, samples were pressure-filtered (99.99% N_2) directly after recovery onboard through 0.2 μm Nuclepore polycarbonate (PC) membrane filters in a Sartorius filtration unit installed in a laminar flow bench, acidified with suprapure HCl to pH ∼ 1.7 (final concentration 0.024 M HCl) and stored in acid-cleaned polyethylene (PE) bottles at 4°C until further analysis. Directly upon recovery of the TMR, the GO-FLO bottles were transported into a class-100 clean container fitted with a HEPA (High Efficiency Particulate Air) filter system. Samples were subsequently pressure-filtered (0.5 bar of 0.1 μm filtered N_2) through 0.2 μm cartridge-filters (AcroPak, Supor), acidified to pH ∼ 1.7 with quartz distilled HCl (final concentration 0.024 M HCl) and stored in acid-cleaned PE bottles at 4°C until further analysis. On shore, seawater samples for trace metals were extracted with an offline seaFAST system (Elemental Scientific) for matrix removal and pre-concentration, prior to analysis with high-resolution sector field inductively coupled plasma—mass spectrometry (HR-SF-ICP-MS, Thermo Finnigan Element 2), largely following the procedures as described by Gerringa et al. (2020). Briefly, a volume of 15 mL sample was pipetted into an acid cleaned FEP vial (Nalgene) and hydrogen peroxide (Merck Suprapur) was added at a final concentration of 10 μmol/L. Subsequently, the samples were digested for 4 h in a home-made UV box after which 10 mL was pre-concentrated using a seaFAST offline pre-concentration system, using Nobias PA1 resin as a pre-concentration column (Lagerström et al., 2013; Bown et al., 2017; Gerringa et al., 2020). Samples were eluted with 1 mL of 1.5 M teflon distilled HNO_3, resulting in a pre-concentration factor of 10. The elution acid contained rhodium as an internal standard to correct for any sensitivity drift of the ICP-MS during analysis. The ion beam intensity of rhodium (as ^{103}Rh) was analyzed in both low resolution and high resolution, ^{208}Pb, ^{111}Cd, and ^{139}La were measured in low resolution, ^{55}Mn, ^{56}Fe, ^{59}Co, ^{60}Ni, ^{63}Cu, and ^{66}Zn were measured in medium resolution. The system was calibrated following the standard addition approach, i.e., a homemade multi-elemental stock standard containing all elements of interest with natural isotopic abundances was added to natural seawater containing low concentrations of metals. Seven standard additions were used for the construction of the calibration curve, where the maximum standard additions were comparable to maximum concentrations in the marine environment. The recovery was verified in every analytical run by comparing the slope of the seawater calibration curve (multi-element standard added to seawater) to the slope of an eluent calibration curve (multi-element standard added directly to the elution acid) after Biller and Bruland (2012) and recoveries were >95%. Blank contributions from the sample handling, pre-concentration and analysis steps were determined by analyzing acidified MQ water (∼1.8 pH) as a sample.

The accuracy and precision of the measurements were determined by measuring the certified reference material CASS-6 from the National Research Council Canada along with the samples. The accuracy for CASS-6 was within ± 5 % of the reference values, except for Cu (+7%), Ni (+8%), and Cd (+12%) (**Supplementary Table 2**). The blanks and limit of detection (**Supplementary Table 2**) were much lower than the observed concentrations.

Macronutrients

For the analysis of macronutrients sample aliquots from the CTD and the TMR casts were immediately filtered with 0.45 μm surfactant-free cellulose acetate (SFCA) syringe filters into high density polyethylene (HDPE) vials. After filtration 150 μL $HgCl_2$ solution (67 mM) was added to 25 mL sample volume (final concentration 0.4 mM $HgCl_2$) to stop biologic activity and samples were stored at 4°C in the dark until further analysis. Within 3 days after collection, samples were analyzed for NO_x, PO_4, and SiO_2 directly on board using colorimetric methods on a 96 well microplate spectrophotometer (Multiscan GO, Thermo Scientific). NO_x was analyzed as described in Schnetger and Lehners (2014), PO_4 concentrations were analyzed using the general method of O'Dell (1993) and the concentrations of dissolved SiO_2 were quantified by applying the method of Grasshoff et al. (1999) (**Supplementary Table 2**).

Noble Gases

Noble gas samples for subsequent analysis in the home laboratory were taken with the CTD water sampler to determine the concentrations of primordial helium (He) in the non-buoyant water column plume. Individual samples were drawn directly after recovery into gas-tight copper tubes, carefully avoiding air contamination by gas bubbles. Samples were analyzed for content of ^{3}He and ^{4}He isotopes at the mass spectrometric facility of the University of Bremen (Germany) with a combination of a high-resolution sector field mass spectrometer and a quadrupole mass spectrometer (Sültenfuß et al., 2009). Total errors based on the instrument performance and standard reference samples for ^{3}He, ^{4}He and Ne concentrations were below 2, 1, and 1%, respectively. Hydrothermally sourced primordial He is characterized by an excess of the isotope ^{3}He. Thus, values are reported as δ^3He (in %) (**Supplementary Table 2**), defined as $(^3He/^4He)/R_a - 1$, the fractional deviation of the ^{3}He/^{4}He ratio in samples from that of air ($R_a = 1.384 \times 10^{-6}$).

Current Measurements

Direct current measurements were carried out using lowered acoustic Doppler current profilers (ADCP). Two TRDI 300 kHz Workhorse Monitor ADCPs were mounted to the CTD water sampler (replacing two of the Niskin bottles) to record full-depth current profiles during the vertical casts, using one upward and one downward looking instrument to increase range and

minimize data gaps. The raw data were processed with an inverse method (Visbeck, 2002) using the barotropic, bottom track and smoothness constraints. The bin length (i.e., the vertical resolution) was set to 10 m, which resulted in an accuracy of 2 cm s^{-1}. As the magnitude of the baroclinic tides induced by the bathymetry of the summits was unknown, tides were not removed from these records. During the time of the measurements, barotropic tidal velocities predicted by the TPXO tidal model at both volcanoes were of the order of 5 cm s^{-1}, with orientation of the tidal ellipses northwest-southeast direction at Brothers, and east-west direction at Macauley (**Supplementary Figure 1**).

Surface currents were geostrophic currents estimated from satellite altimeter data. Here we used the delayed-time all satellites 1/4° grid product produced by AVISO+ (Archiving, Validation and Interpretation of Satellite Oceanographic data) and distributed by the European Union's Earth observation program (Copernicus).

Radium Analysis and Apparent Age Calculation

Dissolved Ra was extracted from water samples with 20 g manganese dioxide coated acrylic fiber to quantitatively adsorb Ra, following the method described in Moore (1976). Radium analysis was done on board with Radium Delayed Coincidence Counters (RaDeCC) (Moore and Arnold, 1996) for both short-lived isotopes ^{223}Ra and ^{224}Ra. The details regarding the measurement procedure, standard measurements, and correction for ^{228}Th activity as well as data processing can be found in Neuholz et al. (2020b). Based on the calculation approach for Brother volcano presented in Neuholz et al. (2020b) assuming horizontal plume advection, we used the same equation to calculate apparent hydrothermal plume ages based on short-lived ^{224}Ra and ^{223}Ra for Macauley.

$$T = -\frac{\ln(AR_x) - \ln(AR_{vent})}{\lambda_s - \lambda_l} \quad (1)$$

This equation requires activity (AR) ratios (^{224}Ra/^{223}Ra). AR_{vent} is the initial AR at the source and AR_x describes the radium isotope ratio (^{224}Ra/^{223}Ra) of a water sample at a certain distance from the vent. λ_s and λ_l are the isotope-specific decay constants of the short (^{224}Ra) and the longer-lived (^{223}Ra) isotope, respectively. The necessary assumptions for the age calculation were assumed to be fulfilled in the hydrothermal environment of Macauley. These assumptions include: (a) the system is dominated by advective transport, (b) the system is in a steady state, i.e., the ratio of ^{224}Ra to ^{223}Ra is constant in the source region, (c) the AR224/223 changes only due to radioactive decay, and (d) the excess ^{224}Ra and ^{223}Ra activity in relation to the open ocean is introduced at the source. Here, hydrothermal venting forms the defined source of short-lived Ra isotopes to the depleted open ocean (e.g., Charette et al., 2015; Kipp et al., 2018). We used the fluid with the "purest" hydrothermal end member composition (i.e., without seawater entrainment) as the initial ^{224}Ra/^{223}Ra end member ratio (AR_{vent} in age equation) (**Supplementary Table 3**) and assumed that the end member fluid remains constant over the studied time period.

Furthermore, we assumed that the neutrally buoyant hydrothermal plume is transported via currents without any contact with bottom water, and consequently, no additional input of Ra is assumed to occur (Neuholz et al., 2020b). Please note, the term "apparent age" is used here, as plume ages were calculated based on the assumption of advective transport and exponential decay only, and may underestimate the actual fluid

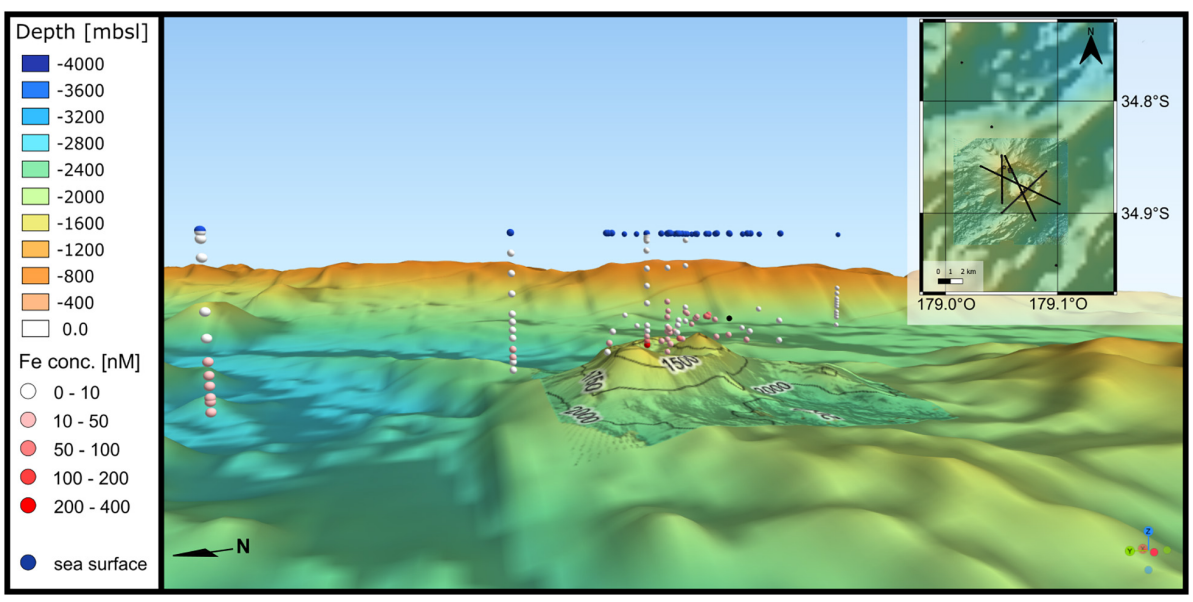

FIGURE 3 | Example screenshot (Brothers, distribution of Fe) of the 3-D model for all discussed trace metals during this study for both volcanoes. The black dots in the small figure on the right show the CTDs and TMRs, while the black lines refer to the conducted tow-yos. mbsl: m below sea level.

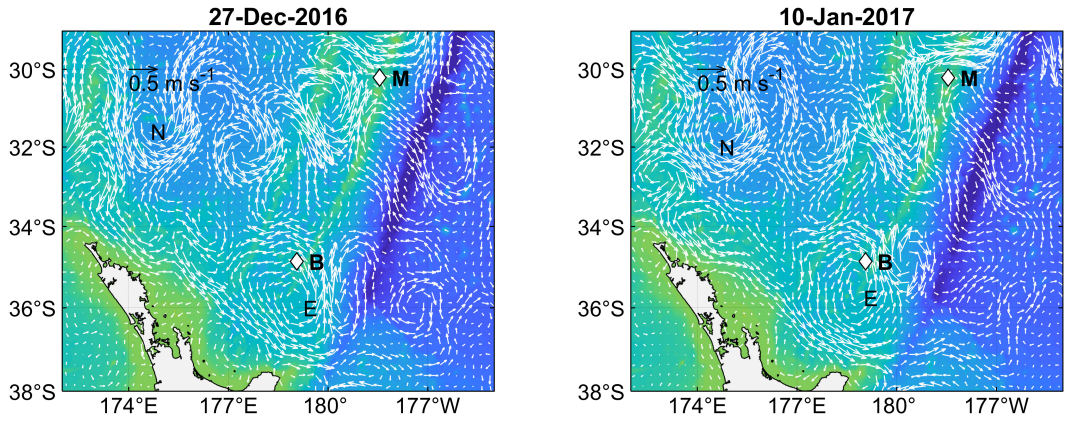

FIGURE 4 | Surface currents derived from satellite-altimeter measurements in the study area on December 27th 2016 (midpoint of the Macauley sampling) and January 10th 2017(midpoint of the Brothers sampling). B stands for Brothers and M for Macauley. The North Cape and East Cape Eddies are shown as N and E.

ages by ignoring mixing processes or diffusive transport (Moore, 2000; Moore and Krest, 2004).

RESULTS

A 3-D model showing trace metal data from all CTDs, TMRs, and tow-yos conducted at Macauley and Brothers (an example is shown in **Figure 3** for Fe at Brothers) can be found under this link: https://www.dropbox.com/sh/90iabpe6y9jwaam/AAC2ab95k10-uTL2s5yky8u6a?dl=0.

Surface Currents

Surface currents derived from satellite-altimeter measurements during the cruise (**Figure 4**) show that the region was dominated by a mesoscale eddy field. On December 27th 2016 (midpoint of sampling at Macauley), the East Auckland Current and the anticyclonic North Cape Eddy were found in about their normal locations, but the anticyclonic North Cape Eddy was west of its mean location (Chiswell et al., 2015). The flow over Macauley was controlled by the confluence of several unnamed eddies, and was weakly to the east. Over the 2 weeks between December 27th 2016 and January 10th 2017 (midpoint of sampling at Brothers), the eddy field evolved, with the East Cape Eddy moving closer to the Brothers so that flow there was to the north-west. These eddies are likely to be barotropic—i.e., they extend deep, and we expect the flows shown in **Figure 4** to approximately represent the flows at the vent depths at the two sites.

Macauley Volcano

Prevailing Currents at Macauley

The surface geostrophic flow on December 27th 2016 (i.e., approximately in the middle of the Macauley sampling period) shows that the region over the Kermadec arc was dominated by the mesoscale eddy field (**Figure 4**). The flow at Macauley was set up by an anti-cyclonic eddy to the north and a pair of cyclonic and anti-cyclonic eddies to the east, so that at the site, the flow was weakly to the east. This weak flow field is broadly consistent with the ADCP measurements made at the site, which were characterized by currents typically less than 10 cm s^{-1} with no preferred direction (**Figure 5**). The maximum current was observed 400 m to the west (CTD 012) with flows of ∼40 cm s^{-1} to the south over depths shallower than 100 m. Below the summit peak, currents rapidly decreased to a few cm s^{-1} with no apparent spatial structure.

Dissolved Trace Metal Distributions at Macauley

At Macauley, two active vent systems dominate. CTD 006 was conducted very close over the shallower 330 m vent, while CTD 012 was conducted directly over the deeper 680 m vent. The respective plume depths are reflected by distinct peaks in turbidity, δ^3He, and dissolved metal concentrations at a water depth of 302 m, especially at CTD 006 (**Figure 6**).

We refer to the depth of these peaks as the maximum plume depth. A comparison of samples taken at the maximum plume depth of CTD 006 (302 m) with samples from a background TMR ∼300 km away collected during GEOTRACES cruise GP13 (Station 28, sampled in 298 m water depth) results in enrichment factors for Zn, Mn, Fe, Cu, Ni, Pb, and Cd of 5422, 4067, 2935, 356, 218, 175, and 9.84, respectively. Calculated plume ages reveal younger ages (2.6–7.6 days) close to the source (CTD 006) and older ages (13.8–18.1 days) with increasing distance from the vent (CTD 012) (**Supplementary Table 3**).

Macronutrient Dispersal at Macauley

While PO_4 and SiO_2 show a clear peak at 302 m at CTD 006, correlating well with the δ^3He and turbidity signals, NO_x does not show this signature (**Figure 6**). No increased macronutrient concentrations were observed 400 m away from the source at CTD 019.

Overall concentrations of NO_x and PO_4 at 302 m are nearly constant at all three CTD casts (except for a slight increase in the NO_x concentration at CTD 019 at 276 m).

SiO_2 showed a clear increase in concentration close to the source at CTD 006 of up to 15 μM, compared to concentrations

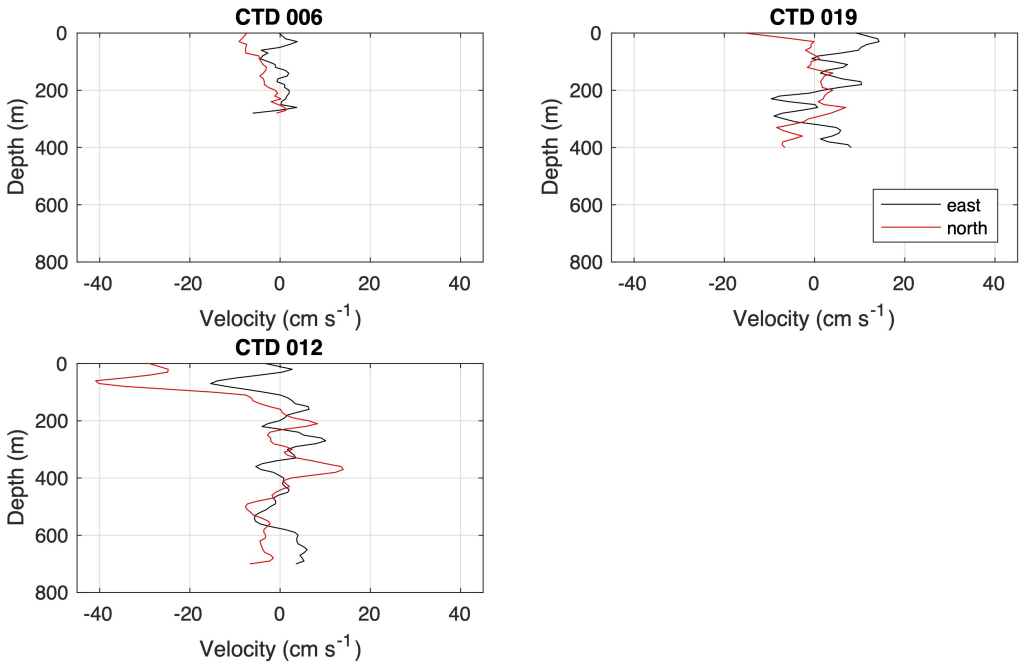

FIGURE 5 | *In situ* currents from lowered ADCP at Macauley. Black denotes east-west velocity (positive to the east), red is north-south velocity (positive to the north).

below the limit of detection (0.1 μM) at shallower depths, or at the same depths at CTD 019 and CTD 012 (**Figure 6** and **Supplementary Table 2**). Despite this enrichment, all three macronutrients follow the typical nutrient-shape depth profile.

Brothers Volcano

Prevailing Currents at Brothers

During the time Brothers was sampled (mid-January 2017), the East Cape Eddy was centered to the southwest of Brothers (**Figure 4**). The satellite-derived surface flow is consistent with the ADCP measurements that revealed a strong north-northwest directed current of up to 35 cm s^{-1} at the surface over the Brothers (**Figure 7**). On the flanks of the Brothers (CTDs 053 and 054), and over the caldera (CTD 058), the ADCP data show that the flow was reasonably barotropic with zonal and meridional components 20–30 cm s^{-1} that reached down to the summit of the volcano, and only vanished within the caldera below the rim at 1550 m (**Figure 7**). Further to the north (CTD 082), the flow was more surface intensified, with stronger surface currents of about 80 cm s^{-1}, also directed to the northwest.

Dissolved Trace Metal Distributions at Brothers

Most of the active hydrothermal venting along the northwest caldera wall appears at ∼1,600 m (de Ronde et al., 2011; Kleint et al., 2019). The depth of the high-temperature vents is reflected by strong turbidity signals and δ^3He peaks at CTDs 053 and 054 (**Figure 8**). A comparison of samples taken in the maximum plume depth (1549 m) of CTD 053 with background samples collected during GEOTRACES cruise GP13 (Station 28, sampled in 1583 m) results in enrichment factors for Mn, Fe, Zn, Pb, Ni, Cd, and Cu of 277, 77.3, 6.41, 2.76, 0.98, 0.83, and 0.39, respectively.

At CTD 058, δ^3He and dissolved trace metal peaks mirror the depth of the active vents at the cone site between 1200 and 1300 m depth (Kleint et al., 2019). Here, samples taken in the maximum plume depth (1229 m) compared to the background sample taken during GP 13, ∼ 280 km away from CTD 053 (Station 28, sampled in 1386 m water depth) reveal enrichment factors for Mn, Fe, Co, Ni, Zn, Cd, Cu, and Pb of 97.4, 27.0, 2.84, 0.93, 0.51, 0.40, and 0.19 respectively.

Ten km southeast outside the caldera, at TMR 070, all dissolved trace metal profiles show a peak at ∼1450 m, the depth of one of the two identified vent sources. Generally, except for Co, which stays nearly constant, the trace metal concentrations increase with depth. At TMR 060 taken 6 km to the northwest of the caldera, a small increase in dissolved metal concentrations, except for Co and La, is visible at 1,450 m. At TMR 083, taken 12 km northwest of the caldera, δ^3He shows increased values with depth, with maximum values between 1,300 and 1,600 m. At the same time, trace metal levels are slightly enriched in these depths, compared to shallower layers, with peaks for Mn, Fe, and Zn at 1450 m superimposed on the general increase with depth and another stronger Fe peak at 1,600 m.

Macronutrient Dispersal at Brothers

The patterns of the macronutrients PO_4, SiO_2, and NO_x do not seem to be affected by the active hydrothermal vents in the caldera (**Figure 9**). The lateral concentrations throughout the six different CTDs and TMRs show the typical increase in concentration with depth. Concentrations at depths shallower than 250 m were below the limit of detection.

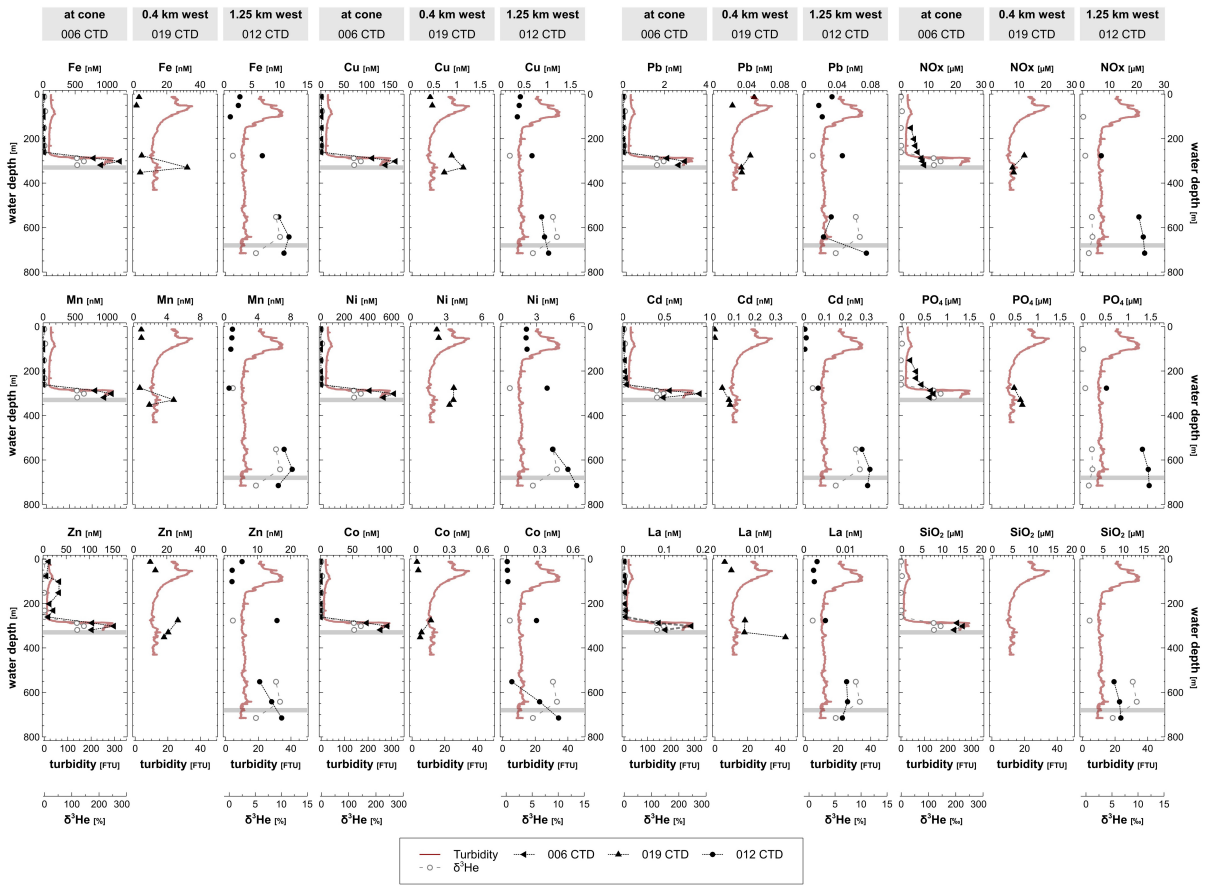

FIGURE 6 | Dissolved metal concentrations of Fe, Mn, Zn, Cu, Ni, Co, Pb, Cd, and La, as well as macronutrient concentrations NO_x, PO_4, and SiO_2 from three CTD casts at Macauley. Also shown are δ^3He and turbidity data. No δ^3He data are available for CTD 019. Horizontal gray bars CTDs 006 and 012 indicate depths of the respective hydrothermal vent sources (Kleint et al., 2019).

DISCUSSION

Hydrothermal Plumes and Prevailing Currents at Macauley and Brothers

The hydrothermal plume maxima are identified by distinct turbidity and δ^3He maxima, and increased dissolved metal concentrations at ∼300 and ∼680 m at Macauley, and between ∼1,200 and 1,300 m, and at ∼1,600 m at Brothers. Another pronounced shallower turbidity signal (∼ 40 FTU), visible at both volcanoes between 50 and 100 m is most likely a result of the deep chlorophyll maximum, as already seen in that area by Ellwood et al. (2018) and is probably not related to hydrothermal input, as neither δ^3He nor metal concentrations are elevated at these depths. While the measured currents at Macauley are weak (10 cm s^{-1}) with no preferred direction (**Figure 5**), dissolved metal data and calculated plume ages suggest a prevailing weak southwest directed current, as CTDs 006, 019, and 012, located along a northeast-southwest transect, show decreasing metal concentrations and older plume ages, derived through Ra isotope analysis, with distance from the vents (**Figure 6**, **Table 1**, and **Supplementary Table 3**). Further evidence of only weak currents at Macauley is also supported by the different plume ages. While the age in the plume maximum at 302 m was calculated to be 7.3 days, a much younger water mass (2.6 days) was calculated below the plume at 319 m water depth (**Supplementary Table 3**). This patchy plume structure is consistent with plume material not being advected far from the vicinity of the vents, and affected only by weak, mostly tidal, currents, with no strong persistent background flow.

At Brothers, current measurements agree with the range of previously reported current speeds at Brothers (Wright, 2001; Lavelle et al., 2008), and revealed strong currents of up to 50 cm s^{-1} magnitude in north-northwest direction (**Figures 7**, **8**), which were consistent with the satellite-derived surface velocity, indicating the influence of the East Cape Eddy on the plume dynamics at the time of the cruise. The current to the north west is confirmed by our dissolved trace metal data, as the CTD and TMR casts 070, 058, 053, 054, 060, and 083 follow a 24 km long southeast-northwest transect over the caldera at Brothers, with stronger hydrothermal signal

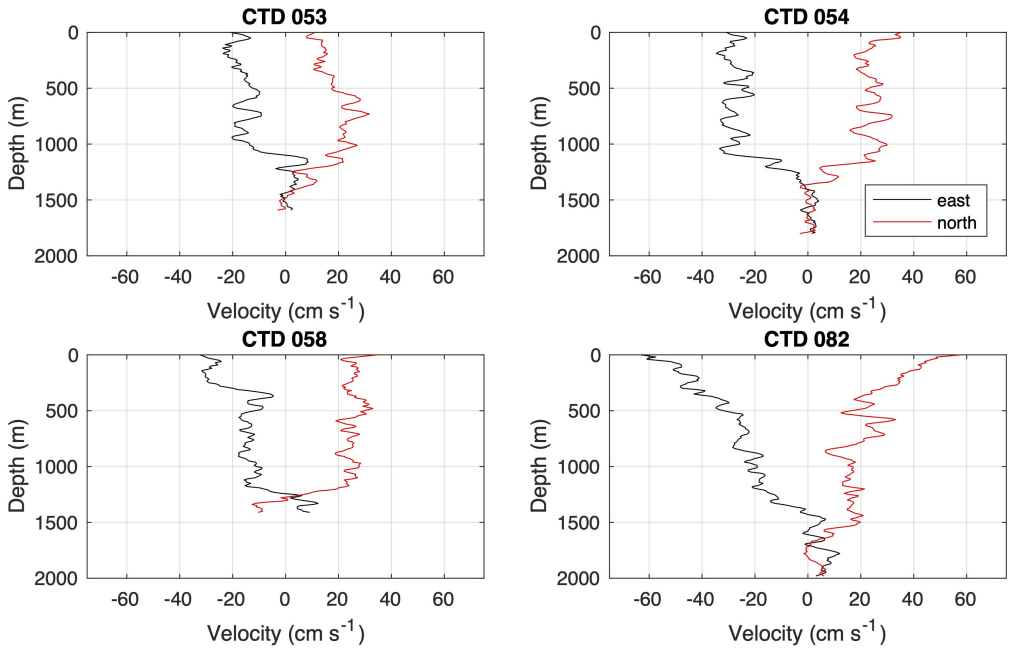

FIGURE 7 | *In situ* currents from lowered ADCP at Brothers. Black denotes east-west velocity (positive to the east), red denotes north-south velocity (positive to the north). CTD 082 was conducted at the same location and on the same day as TMR 083.

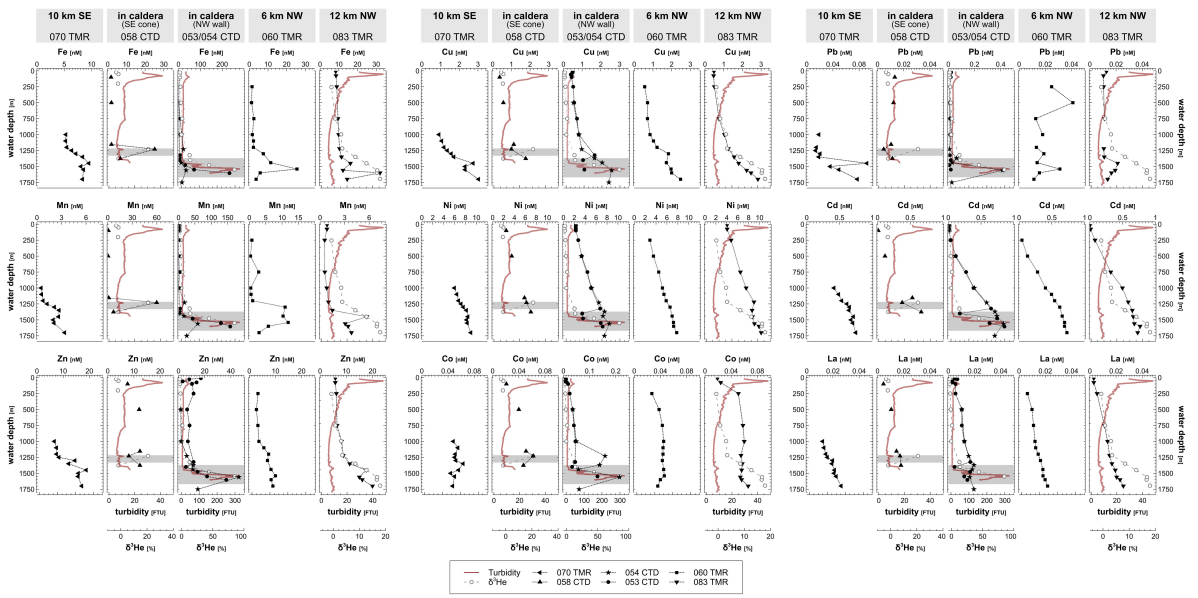

FIGURE 8 | Dissolved metal concentrations of Fe, Mn, Zn, Cu, Ni, Co, Pb, Cd, and La for six different CTD casts over the Brothers volcano, together with δ ^{3}He and turbidity data. No δ ^{3}He and turbidity data are available for TMR 070 and TMR 060. δ ^{3}He and turbidity data for TMR 083 was taken from CTD 082, which was conducted at the same location and same day. The gray areas in the plots of the CTDs taken within the caldera indicate depths of the hydrothermal vent sources (Kleint et al., 2019).

toward the northwest, compared to the southwest, especially for Fe and Mn (**Figure 8**). Also, calculated plume ages, based on Ra isotopes, support a northwest directed current (Neuholz et al., 2020a).

Macronutrients in the Hydrothermal Plumes of Brothers and Macauley

Macronutrients generally showed typical vertical profiles with very low concentrations in the surface layer due to biological

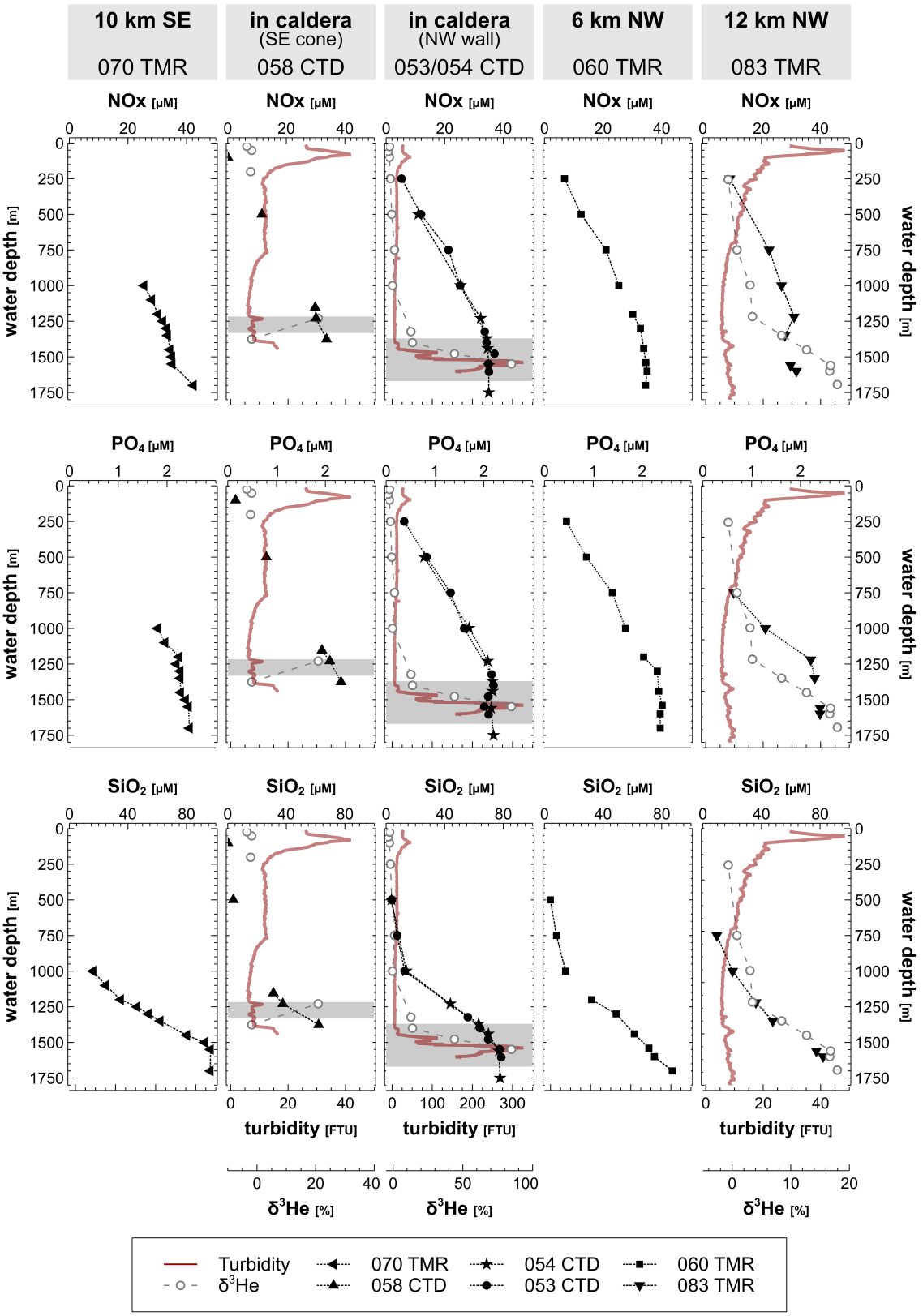

FIGURE 9 | NO_x, PO_4, and SiO_2 data for six different CTD casts over the Brothers volcano, together with δ^3He and turbidity data. No δ^3He and turbidity data are available for TMR casts, i.e., TMR 070 and TMR 060. δ^3He and turbidity data for TMR 083 were taken from CTD 082, which was conducted at the same location and same day. The gray areas in the plots of the CTDs taken within the caldera indicate depths of the hydrothermal vent sources (Kleint et al., 2019).

TABLE 1 | Element/Fe ratios [mol/mol], δ^3He, turbidity values, and Ra-isotope derived plume ages in the plume maximum at ∼300 m for three CTD casts at Macauley with distance from the source.

CTD	Depth [m]	Distance from source [km]	δ^3He [%]	Average turbidity [FTU]	Plume age [days]	Mn/Fe	Zn/Fe	Cu/Fe	Co/Fe	Ni/Fe	Pb/Fe	Cd/Fe	La/Fe
006	302	At cone	145	270	7.3	0.895	0.128	0.136	0.088	0.519	0.0025	0.0008	0.00014
019	330	0.40	–	13.8	9.5	0.150	0.646	0.035	0.002	0.112	0.0010	0.0023	0.00023
012	277	1.25	0.700	10.5	–	0.088	2.320	0.098	0.039	0.566	0.0067	0.0100	0.00075

The fluid source is at ∼ 330 m depth (Kleint et al., 2019). Turbidity values were averaged for each sampling depth. No δ^3He data is available for CTD 019. No water age is available for CTD 012 at 277 m.

uptake, and continuously increasing concentrations with depth due to regeneration. No clear hydrothermal signatures were found in our study, only PO_4 and SiO_2 showed a pronounced peak at the maximum plume depth at station CTD 006 at Macauley. This peak is not visible for NO_x, neither at the stations further away from the vent nor in close vicinity of Brothers (**Figures 6**, **9**). Therefore, we assume that PO_4 and SiO_2 are both released by the Macauley vent systems, followed by their rather quick removal from the plumes and the water column by coprecipitation onto Fe-oxyhydroxides or by biological uptake (Wheat et al., 1996). At Brothers, a minimum signal of PO_4 around 1500 m at the northwest wall of the caldera (CTD 053/054) may indicate inclusion of PO_4 in Fe oxyhydroxide particles as was shown for other hydrothermal systems (Bennett et al., 2009), however, no apparent PO_4 removal is observed in other profiles in our study. Overall, macronutrients show neither a significant hydrothermal source nor a sink in both study areas during the investigated timeframe, which is in line with GEOTRACES data from the Australian/New Zealand transect GP13 over the Kermadec arc at 32°S (Ellwood et al., 2018), indicating that the hydrothermal signature of macronutrients is negligible on a basin scale, but may be influencing local nutrient distributions.

Trace Metal Signatures in the Macauley Plumes

The hot fluids (up to 112°C) of the Macauley vent are, despite its shallow water depth, rich in sulfide (up to 10.4 mM), and due to their low pH of 1.2 also rich in dissolved metals (up to 1.71 mM Fe, 0.868 mM Mn, 0.243 mM Zn, 1.23 μM Pb, and 77.5 nM La; total REE: 2.26 μM) (Kleint et al., 2019). The high sulfide concentration leads to H_2S/Fe ratios of up to 8.04 in the fluid. In the early plume, a large fraction of dissolved metals, such as Fe, Zn, Cu, and Co, is usually rapidly lost, as these metals react with prevalent sulfides to form settling sulfide mineral particles (Yücel et al., 2011). A fraction of the hydrothermally derived dissolved trace metals may also form sulfide nanoparticles, which do not settle, but can be transported within the non-buoyant hydrothermal plume with long residence times (Yücel et al., 2011; Gartman et al., 2014; Findlay et al., 2019). In the plume maxima (determined by max. turbidity concentrations, see **Table 1**, CTD samples: 006, 019, and 012) δ^3He, turbidity and dissolved trace metal concentrations generally decreased with distance from the vent with CTD 006 > 019 > 012 (**Figure 6**).

The normalization of trace metals to Fe, with Fe as the primary particle-forming element, was performed at all stages of plume dispersion, with the intent to use element/Fe ratios (see **Table 1**) to reveal relative enrichments or depletions of common elements in different stages of plume dispersal. Although decreasing dissolved concentrations were measured with distance from the source for all elements, element/Fe ratios of Zn, Cd, and La increase with distance (**Table 1**). Specifically for Zn, one other study (Haalboom et al., 2020) has reported similar trends. A possible reason for the increasing Zn/Fe ratios with distance is the higher solubility of Zn in seawater compared to that of Fe, meaning that Fe precipitates faster during plume evolution compared to Zn (Liu and Millero, 2002). Nevertheless, organic complexations of both Zn and Fe, have been observed in various plumes (Bennett et al., 2008; Kim et al., 2015). However, on global ocean scales, the transport of hydrothermally derived Zn is far from understood and study outcomes generally disagree widely. While Conway and John (2014) state that the Mid Atlantic Ridge (MAR) hydrothermal vents are not a source of Zn to the ocean, Roshan et al. (2016) demonstrated for the tropical South Pacific (GP16) that hydrothermal Zn is transported from the East Pacific Rise through the central South Pacific basin. Our study site at Macauley agrees with the latter study, with Zn displaying a clear transport from the source (**Table 1**).

The increasing Cd/Fe ratio with distance from the source (**Table 1**) may be explained by the re-dissolution of Cd from plume particles in the non-buoyant plume, which is in agreement with studies form the MAR (James and Elderfield, 1996), while increasing La/Fe ratios probably result from continuous scavenging of La from ambient seawater onto < 0.2μm Fe-oxyhydroxide colloids, which would pass the filter and end up in the filtrate (Elderfield and Greaves, 1982; Edmonds and German, 2004).

The strong decrease of chalcophile elements, such as Cu and Co, Ni, and Pb from CTD 006 toward CTD 019, only 400 m away, indicates a rapid removal from the dissolved phase of the plume, most likely as particulate sulfides, as indicated by the high fluid H_2S concentration and H_2S/Fe ratios at Macauley (Cave et al., 2002; Edmonds and German, 2004; Haalboom et al., 2020).

While Noble et al. (2015) did not see Pb in the neutrally buoyant plume at TAG hydrothermal vent field, due to complete precipitation into near-field sediments, we observed elevated Pb concentrations in the neutrally buoyant plume maxima in all Macauley CTD casts. This trend indicates that the Macauley vents are a source of dissolved Pb. The trends observed at Macauley for Cu, Ni, Co, and Pb suggest a fast formation of larger sulfide

particles (> 0.2 μm) in the early stage of plume dispersion, removing large quantities of these dissolved metals from the plume. Interestingly, the ratios of Cu, Co, Ni and Pb to Fe increase again at CTD 012, 1.25 km away from the vent, likely due to the oxidative dissolution of metal-sulfide particles and colloids, as previously observed in rising plumes at the MAR (Sarradin et al., 2009). Here, iron oxyhydroxides are presumed to become more important, scavenging dissolved elements from the plume and surrounding seawater (Haalboom et al., 2020).

Another aspect of keeping Fe and Zn, Cu, Ni, Co and also La in solution is by the complexation of organic ligands (van den Berg, 2000; Liu and Millero, 2002; Sander and Koschinsky, 2011; Schijf and Byrne, 2021). Ambient organic metal binding ligands are omnipresent in the marine environment and have been shown to be produced by hydrothermal vents themselves and their associated ecosystems, especially in diffuse venting areas and buoyant plumes, by microbial activity and degradation processes of organic matter (Lough et al., 2019a).

Organic ligands of different sources will readily complex the hydrothermally sourced trace metals either directly in the buoyant plume, or later in the non-buoyant plume, leading to increased fluxes of dissolved trace metals above their inorganic thermodynamic solubility (as shown for the stabilization of Fe, Bennett et al., 2008; Sander and Koschinsky, 2011; Hawkes et al., 2013; Kleint et al., 2016). Organic metal complexation at Macauley was not investigated in this study but is the topic of another manuscript currently in preparation.

Overall, a concert of different inorganic and organic reactions are responsible for the trace element distribution and speciation in hydrothermal plumes and which of these processes dominates depends on many criteria including the concentration of H_2S, Fe, and the presence of biogenic organic ligands. The complexity of this aspect requires further systematic investigations.

Trace Metal Signatures in the Brothers Plumes

The fluids at Brothers volcano are highly diverse and reach from typical high temperature black smoker type fluids at the northwest caldera wall (∼1,600 m) to more diffuse and clear smoker fluids at the upper and lower cone site (∼1,200–1,300 m, Kleint et al., 2019). These different vent fields are reflected in the different CTD casts by pronounced peaks in turbidity, δ^3He, and trace metal concentrations at the respective vent depths (**Figure 8**). Plume depths determined in this study agree well with previous studies at the Brothers volcano system (Walker et al., 2018). Studied vents are located inside the caldera, where relatively slow currents of only 5 cm s^{-1} (Neuholz et al., 2020b) have been measured. Strong north-northwesterly currents were detected above the caldera rim (>50 cm s^{-1}) at ∼1550 m, potentially transporting some of the hydrothermal plume material out of the caldera into the distal ocean (**Figure 7** and Neuholz et al., 2020a). This outward transport is confirmed by both our trace metal and δ^3He data, which display hydrothermal signals at a depth of ∼1,600 m, 12 km northwest of the caldera, presumably originating from the vents at the northwest caldera wall (**Figure 8**). The fluids from the caldera wall vents are rich in dissolved Fe (up to 12.4 mM, average Fe is 5.55 mM, n = 22) at a maximum concentration of 5.91 mM H_2S (average H_2S is 0.948 mM, n = 19; Kleint et al., 2019). Due to the low H_2S/Fe ratio (as low as 0.085) a significant amount of Fe is assumed to precipitate more slowly via oxidation, forming Fe oxyhydroxides instead of the rapid Fe sulfide formation suggested at Macauley and discussed in section "Trace Metal Signatures in the Macauley Plumes." This process is important, as the respective formation of both oxyhydroxides and sulfides not only controls the fate of dissolved Fe and many other trace elements in the hydrothermal near and far field hydrothermal plume, but it also affects the long-range dispersal of Fe and its biological uptake in the open ocean. While many metals may precipitate as discrete sulfide phases when the sulfide content is high in the fluid, a lower sulfide concentration and Fe oxyhydroxide formation could mean that metals such as Ni, Co, Zn, Cu, Cd, and Pb stay in solution longer and only slowly decrease when sorption on newly formed Fe oxyhydroxides becomes relevant (Baker and Massoth, 1987; Mottl and McConachy, 1990; Statham et al., 2005; González-Santana et al., 2020; Roshan et al., 2020).

Mn/Fe ratios in the plume at ∼1,600 m (**Table 2**), show similar trends as for Macauley, that is, a continuous decrease with distance from the source toward the northwest. Zn/Fe ratios increase from CTD 053 to TMR 083 at 12 km distance, which agrees with increasing Zn/Fe ratios at Macauley. The same trend was observed for Cu/Fe, Ni/Fe, Cd/Fe, and La/Fe ratios (**Table 2**). The increase is, however, most prominent closest to the source in the caldera compared to no or only a minor increase in the TMRs further outside the caldera. This trend is different from the one shown at Macauley and may indicate that—due to low H_2S/Fe ratios at Brothers NW caldera wall in contrast to higher H_2S/Fe ratios at Macauley—a significant fraction of these elements precipitates more slowly as Fe-oxyhydroxides, instead of rapid metal-sulfide formation. Interestingly, in contrast to Macauley, at Brothers the Co/Fe ratios stay constant from inside

TABLE 2 | Element/Fe ratios [mol/mol] at plume depth (∼1,550–1,600 m) in vertical CTDs and TMRs taken along a transect within the caldera (CTD 053), toward 6 km (TMR 060) and 12 km to the northwest (TMR 083) outside the caldera of the Brothers volcano.

CTD/TMR*	Depth [m]	Distance from source [km]	δ^3He[%]	Average turbidity [FTU]	Mn/Fe	Zn/Fe	Cu/Fe	Co/Fe	Ni/Fe	Pb/Fe	Cd/Fe	La/Fe
053–04	1,549	At NW wall	84.8	255	1.818	0.307	0.016	0.0018	0.096	0.0003	0.009	0.0002
060–03*	1,540	6	–	–	0.466	0.394	0.077	0.0018	0.283	0.0012	0.027	0.0007
083–02*	1,600	12	18.0	8.43	0.107	0.501	0.077	0.0017	0.309	0.0005	0.024	0.0007

*No δ^3He data and turbidity data are available for TMR 060. *Refers to TMR stations.*

the caldera all the way toward 12 km to the NW, indicating a close linkage of the processes governing the dissolved phase of both elements at Brothers. Pb/Fe ratios show a different trend at Brothers than at Macauley, with an initial increase followed by a decrease (**Tables 1**, **2**). This trend is in line with the importance of H_2S for the long-range transport of Pb and indicates that at Brothers, Pb is lost from the non-buoyant plume by co-precipitation onto Fe oxyhydroxides or by scavenging onto Mn oxides (Gartman and Findlay, 2020).

The cone site shows active venting at 1,200–1,300 m depth (Kleint et al., 2019). The plume signals from this site are visible in the data from CTD 058, taken in close vicinity to the cone site (**Figure 8**), by clear δ^3He and turbidity anomalies, as well as elevated metal concentrations for Fe, Mn, Co, and La. Interestingly, metal concentrations for Zn, Cu, Pb and Cd are depleted in the plume compared to concentration below and above the plume (**Figure 8**). This decrease in the plume could be caused by a rapid loss of these chalcophilic elements from solution via the formation of sulfide minerals large enough to settle, which agrees with high H_2S/Fe ratios. Maximum fluid H_2S and dissolved Fe concentrations of 4.49 mM and only 41 μM, respectively (sample 045 ROV 3F, Kleint et al., 2019), result in the highest H_2S/Fe ratios (110), seen in this study even much higher when compared to Macauley (8.04) and certainly to the Brothers NW Caldera Wall vents (0.085). The weak plume signal at 1450 m water depth seen in TMR 070, 10 km SE outside the caldera, most likely results from other active vents in the area (**Figure 1**), as the prevailing measured currents during our cruise do not support a transport toward the southeast (**Figures 7**, **8**).

CONCLUSION

This study evaluated, for the first-time, trace metal dynamics of Mn, Fe, Co, Ni, Cu, Zn, Cd, La, and Pb in different hydrothermal plumes of the Kermadec arc, in the southwest Pacific Ocean. Our results demonstrate that hydrothermal plumes above volcanic arcs provide a dynamic and diverse environment, and that the fluid chemistry (particularly element enrichment factors) plays a major role in the transport and stabilization of hydrothermally derived trace metals.

Magmatic hydrothermal fluids, and black-smoker type fluids originating from water-rock interaction, each produce distinct plume signatures with different elemental ratios. This diversity has consequences for the behavior of these elements, implying that the two different types of hydrothermal systems, even though often occurring in close vicinity to each other, such as in our study, may have different influences on the local and distant trace metal biogeochemical cycles in the ocean.

At the magmatically influenced Macauley site and the Brothers cone site, the transport of trace metals most likely takes place via suspended or dissolved metal-sulfide species, as indicated by relatively high H_2S/Fe fluid ratios (8.04 and 110, respectively). The low pH (especially of the Macauley fluids) facilitates the release of high dissolved trace metal concentrations such as Fe and Zn, which are, in the non-buoyant plume, most likely not only stabilized by sulfide nanoparticles but also by organic ligands.

At the black-smoker type vents (the northwest caldera wall of Brothers), Fe oxyhydroxides seem to dominate over sulfide nanoparticles (low H_2S/Fe fluid ratio of only 0.085) and thereby stabilize dissolved trace metals in the hydrothermal plumes, probably together with organics. We traced the plume at Brothers volcano over a distance of 12 km from the active vents and we could show that especially elements such as Fe, Mn, Zn, Ni but also Cd and Pb are still enriched at this distance compared to values above and below the plume depth and to the background station. This significant hydrothermal signature in the near-to-medium-scale field around these vents highlights the likely importance of hydrothermally derived trace metals in shaping larger scale biogeochemical cycles.

The shallow Macauley system and the deeper Brothers systems, both release large amounts of trace metals in relatively shallow water depth. Our data, especially from the Macauley system, suggests that these shallower submarine volcanoes may impact biological activity in the photic zone by providing micronutrients to the oceans on a local scale as observed recently in the Southern Ocean (Schine et al., 2021). At Brothers, all trace metal concentrations were below the 95% level of protection threshold of species of the Australian and New Zealand Guidelines for Fresh and Marine Water Quality (ANZECC), while at Macauley concentrations for Cu and Co were up to 7.8 and 6.2 times above the 95% threshold (ANZECC and ARMCANZ, 2000), respectively (CTD 006, **Supplementary Table 2**). Nevertheless, an actual toxicity assessment in deep sea environments is challenging due to the lack of (i) organisms tested at relevant conditions (pressure, pH, temperature) and (ii) Cu and Co speciation values (i.e., determination of organic complexation) which are known to be much better proxies of trace metal bioavailability and thus toxicities than total dissolved values. A more detailed discussion of potential toxicities at Macaulay is out of the scope of this study. Macronutrients at Brothers and Macauley did not show a major hydrothermal source or sink, indicating that even if the hydrothermal signature influences nutrient distributions on local scales, it is negligible on a basin scale. To elucidate these biogeochemical interactions in more detail, speciation analyses are needed to assess the role of organic ligands on the stability and bioavailability of these metals in these environments.

Kleint et al. (2019) showed how spatially and temporally diverse and variable the different volcanic systems at the Kermadec arc are with respect to their fluid chemistry. Our data show the same variability in the plumes above the vents. These plumes are transported and mixed laterally and vertically by the ocean circulation, underlining the importance of the local eddy fields for the dispersal of plume material. Variability in the mesoscale eddy field makes it very difficult to quantify the importance of such island arc systems (making up about 25% of hydrothermal vent fields, Beaulieu et al., 2013) in global oceanic dissolved trace metal distributions. We therefore recommend future high-resolution sampling and systematic investigations of plumes at different hydrothermal systems (mid-ocean ridges, arc and back arc systems), including time series, chemical speciation and size fractionation in conjunction with data on biological

productivity for a more holistic picture of such systems. Each individual study would contribute to a better understanding of the fate and bioavailability of hydrothermally derived trace metals in the ocean and a systematic classification of the prevailing processes governing the trace element transportation associated with hydrothermal activity is envisioned to greatly improve biogeochemical models of the current and future ocean.

DATA AVAILABILITY STATEMENT

The original contributions presented in the study are included in the article/**Supplementary Material**, further inquiries can be directed to the corresponding author/s.

AUTHOR CONTRIBUTIONS

CK, AK, BS, MW, and SS carried out the conceptualization of the study. CK as well as RN, BS, MW, SS, RZ, and AK were responsible for the collection of all hydrothermal plume samples at sea during SO253. CK, RZ, RM, and PL performed trace metal analysis. RN and BS were responsible for macronutrient data and plume age calculations. MW generated He and current data. Interpretation and discussion of the data was mainly performed by CK, RZ, SS, and MW including contributions by RN, BS, LK, SC, RM, PL, and AK. All authors contributed to and approved the final version of this manuscript.

FUNDING

Funding of this project (03G0253) was provided by the BMBF (German Federal Ministry of Education and Research) and was gratefully acknowledged. CK was partially funded by the Cluster of Excellence 2077 University of Bremen, MARUM (project number: 390741603). This study received financial support from the University of Otago Grant.

ACKNOWLEDGMENTS

We thank Captain L. Mallon and his crew for their skilled support of the scientific work onboard the R/V Sonne. Cornel de Ronde and Sharon Walker are thanked for their excellent and everlasting support during CTD deployments. We are thankful to Janis Thal for generating and providing high-resolution bathymetric maps and to Carola Lehners from the University of Oldenburg/ICBM for macronutrient analyses onboard. The New Zealand authorities are acknowledged for permission to work along the Kermadec arc. We are also grateful to the team of the GEOTRACES transect GP13 led by PIs Boyd and Bowie for the permission to use the trace element data of station 28. We thank AVISO^{+} for the free use of the satellite-derived surface velocities.

SUPPLEMENTARY MATERIAL

The Supplementary Material for this article can be found online at: https://www.frontiersin.org/articles/10.3389/fmars.2021.782734/full#supplementary-material

REFERENCES

ANZECC and ARMCANZ (2000). *Australian and New Zealand Guidelines for Fresh and Marine Water Quality. National Water Quality Management Strategy Paper No 4*.

Ardyna, M., Lacour, L., Sergi, S., D'Ovidio, F., Sallée, J.-B., Rembauville, M., et al. (2019). Hydrothermal vents trigger massive phytoplankton blooms in the Southern Ocean. *Nat. Commun.* 10:2451. doi: 10.1038/s41467-019-09973-6

Baker, E. T., German, C. R., and Elderfield, H. (1995). Hydrothermal Plumes Over Spreading-Center Axes: Global Distributions and Geological Inferences. *Geophysical Monograph Series* 91, 47–71. doi: 10.1029/GM091p0047

Baker, E. T., and Massoth, G. J. (1987). Characteristics of hydrothermal plumes from two vent fields on the juan de fuca ridge, northeast pacific ocean. *Earth Planet. Sci. Lett.* 85, 59–73. doi: 10.1016/0012-821X(87)90021-5

Baker, E. T., Walker, S. L., Embley, R. W., and De ronde, C. E. J. (2012). High-resolution hydrothermal mapping of brothers caldera, kermadec arc. *Econ. Geol.* 107, 1583–1593. doi: 10.2113/econgeo.107.8.1583

Beaulieu, S. E., Baker, E. T., German, C. R., and Maffei, A. (2013). An authoritative global database for active submarine hydrothermal vent fields. *Geochem. Geophys. Geosyst.* 14, 4892–4905. doi: 10.1002/2013GC004998

Bennett, S. A., Achterberg, E. P., Connelly, D. P., Statham, P. J., Fones, G. R., and German, C. R. (2008). The distribution and stabilisation of dissolved Fe in deep-sea hydrothermal plumes. *Earth Planet. Sci. Lett.* 270, 157–167. doi: 10.1016/j.epsl.2008.01.048

Bennett, S. A., Rouxel, O., Schmidt, K., Garbe-Schönberg, D., Statham, P. J., and German, C. R. (2009). Iron isotope fractionation in a buoyant hydrothermal plume, 5°S mid-atlantic ridge. *Geochim. Cosmochim. Acta* 73, 5619–5634. doi: 10.1016/j.gca.2009.06.027

Biller, D. V., and Bruland, K. W. (2012). Analysis of Mn, Fe, Co, Ni, Cu, Zn, Cd, and Pb in seawater using the Nobias-chelate PA1 resin and magnetic sector inductively coupled plasma mass spectrometry (ICP-MS). *Mar. Chem.* 130–131, 12–20. doi: 10.1016/j.marchem.2011.12.001

Bown, J., Laan, P., Ossebaar, S., Bakker, K., Rozema, P., and de Baar, H. J. W. (2017). Bioactive trace metal time series during austral summer in Ryder Bay, Western Antarctic Peninsula. *Deep Sea Res. Part II Top. Stud. Oceanogr.* 139, 103–119. doi: 10.1016/j.dsr2.2016.07.004

Boyd, P. W., and Ellwood, M. J. (2010). The biogeochemical cycle of iron in the ocean. *Nat. Geosci.* 3, 675–682. doi: 10.1038/ngeo964

Bristow, L. A., Mohr, W., Ahmerkamp, S., and Kuypers, M. M. M. (2017). Nutrients that limit growth in the ocean. *Curr. Biol.* 27, R474–R478. doi: 10.1016/j.cub.2017.03.030

Butler, E. C. V., O'Sullivan, J. E., Watson, R. J., Bowie, A. R., Remenyi, T. A., and Lannuzel, D. (2013). Trace metals Cd, Co, Cu, Ni, and Zn in waters of the subantarctic and polar frontal zones south of tasmania during the 'SAZ-sense' project. *Mar. Chem.* 148, 63–76. doi: 10.1016/j.marchem.2012.10.005

Cave, R. R., German, C. R., Thomson, J., and Nesbitt, R. W. (2002). Fluxes to SEDIMENTS underlying the rainbow hydrothermal plume at 36°14'N on the mid-Atlantic ridge. *Geochim. Cosmochim. Acta* 66, 1905–1923. doi: 10.1016/S0016-7037(02)00823-2

Charette, M. A., Morris, P. J., Henderson, P. B., and Moore, W. S. (2015). Radium isotope distributions during the US GEOTRACES north Atlantic cruises. *Mar. Chem.* 177, 184–195. doi: 10.1016/j.marchem.2015.01.001

Chiswell, S. M. (2005). Mean and variability in the wairarapa and hikurangi eddies. *New Zealand. New Zeal. J. Mar. Freshw. Res.* 39, 121–134. doi: 10.1080/00288330.2005.9517295

Chiswell, S. M., Bostock, H. C., Sutton, P. J., and Williams, M. J. (2015). Physical oceanography of the deep seas around new Zealand: a review. *New Zeal. J. Mar. Freshw. Res.* 49, 286–317. doi: 10.1080/00288330.2014.992918

Conway, T. M., and John, S. G. (2014). The biogeochemical cycling of zinc and zinc isotopes in the North Atlantic Ocean. *Global. Biogeochem. Cycles* 28, 1111–1128. doi: 10.1002/2014GB004862

Cotte, L., Omanović, D., Waeles, M., Laës, A., Cathalot, C., Sarradin, P.-M., et al. (2018). On the nature of dissolved copper ligands in the early buoyant plume of hydrothermal vents. *Environ. Chem.* 15:58. doi: 10.1071/EN17150

de Ronde, C. E., Massoth, G. J., Baker, E. T., and Lupton, J. E. (2003). "Submarine hydrothermal venting related to volcanic arcs," in *Volcanic, Geothermal, and Ore-Forming Fluids: Rulers and Witnesses of Processes Within the Earth*, eds S. F. Simmons and I. J. Graham (Littleton, Colo: Society of Economic Geologists. Special publication / Society of Economic Geologists), 91–109. doi: 10.5382/SP.10

de Ronde, C. E. J., Baker, E. T., Massoth, G. J., Lupton, J. E., Wright, I. C., Sparks, R. J., et al. (2007). Submarine hydrothermal activity along the mid-kermadec arc, new zealand: large-scale effects on venting. *Geochem. Geophys. Geosyst.* 8:1495. doi: 10.1029/2006GC001495

de Ronde, C. E. J., Butterfield, D. A., and Leybourne, M. I. (2012). Metallogenesis and mineralization of intraoceanic arcs I: kermadec arc–introduction. *Econ. Geol.* 107, 1521–1525. doi: 10.2113/econgeo.107.8.1521

de Ronde, C. E. J., Hannington, M. D., Stoffers, P., Wright, I. C., Ditchburn, R. G., Reyes, A. G., et al. (2005). Evolution of a submarine magmatic-hydrothermal system: brothers volcano, southern kermadec arc, new zealand. *Econ. Geol.* 100, 1097–1133.

de Ronde, C. E. J., Massoth, G. J., Butterfield, D. A., Christenson, B. W., Ishibashi, J., Ditchburn, R. G., et al. (2011). Submarine hydrothermal activity and gold-rich mineralization at brothers volcano, kermadec arc, new zealand. *Miner. Depos.* 46, 541–584. doi: 10.1007/s00126-011-0345-8

Echeveste, P., Agustí, S., and Tovar-Sánchez, A. (2012). Toxic thresholds of cadmium and lead to oceanic phytoplankton: cell size and ocean basin-dependent effects. *Environ. Toxicol. Chem.* 31, 1887–1894. doi: 10.1002/etc.1893

Edmonds, H. N., and German, C. R. (2004). Particle geochemistry in the rainbow hydrothermal plume, mid-atlantic ridge. *Geochim. Cosmochim. Acta* 68, 759–772. doi: 10.1016/S0016-7037(03)00498-8

Elderfield, H., and Greaves, M. J. (1982). The rare earth elements in seawater. *Nature* 296, 214–219. doi: 10.1038/296214a0

Ellwood, M. J., Bowie, A. R., Baker, A., Gault-Ringold, M., Hassler, C., Law, C. S., et al. (2018). Insights into the biogeochemical cycling of iron, nitrate, and phosphate across a 5,300 km south pacific zonal section (153°E-150°W). *Global Biogeochem. Cycles* 32, 187–207. doi: 10.1002/2017GB005736

Feely, R. A., Trefry, J. H., Lebon, G. T., and German, C. R. (1998). The relationship between P/Fe and V/Fe ratios in hydrothermal precipitates and dissolved phosphate in seawater. *Geophys. Res. Lett.* 25, 2253–2256. doi: 10.1029/98GL01546

Findlay, A. J., Estes, E. R., Gartman, A., Yücel, M., Kamyshny, A., and Luther, G. W. (2019). Iron and sulfide nanoparticle formation and transport in nascent hydrothermal vent plumes. *Nat. Commun.* 10:1597. doi: 10.1038/s41467-019-09580-5

Fitzsimmons, J. N., Boyle, E. A., and Jenkins, W. J. (2014). Distal transport of dissolved hydrothermal iron in the deep South Pacific Ocean. *Proc. Natl. Acad. Sci. U.S.A.* 111, 16654–16661. doi: 10.1073/pnas.1418778111

Fitzsimmons, J. N., John, S. G., Marsay, C. M., Hoffman, C. L., Nicholas, S. L., Toner, B. M., et al. (2017). Iron persistence in a distal hydrothermal plume supported by dissolved–particulate exchange. *Nat. Geosci.* 10, 195–201. doi: 10.1038/ngeo2900

Gartman, A., and Findlay, A. J. (2020). Impacts of hydrothermal plume processes on oceanic metal cycles and transport. *Nat. Geosci.* 13, 396–402. doi: 10.1038/s41561-020-0579-0

Gartman, A., Findlay, A. J., and Luther, G. W. (2014). Nanoparticulate pyrite and other nanoparticles are a widespread component of hydrothermal vent black smoker emissions. *Chem. Geol.* 366, 32–41. doi: 10.1016/j.chemgeo.2013.12.013

GEBCO Bathymetric Compilation Group (2020). *The GEBCO_2020 Grid – A Continuous Terrain Model of the Global Oceans and Land.* Available online at: https://www.gebco.net/data_and_products/gridded_bathymetry_data/

German, C. R., Casciotti, K. A., Dutay, J.-C., Heimbürger, L. E., Jenkins, W. J., Measures, C. I., et al. (2016). Hydrothermal impacts on trace element and isotope ocean biogeochemistry. *Philos. Trans. R. Soc. A Math. Phys. Eng. Sci.* 374:35. doi: 10.1098/rsta.2016.0035

German, C. R., Fleer, A. P., Bacon, M. P., and Edmond, J. M. (1991). Hydrothermal scavenging at the mid-atlantic ridge: radionuclide distributions. *Earth Planet. Sci. Lett.* 105, 170–181. doi: 10.1016/0012-821X(91)90128-5

Gerringa, L. J. A., Alderkamp, A.-C., van Dijken, G., Laan, P., Middag, R., and Arrigo, K. R. (2020). Dissolved trace metals in the ross sea. *Front. Mar. Sci.* 7:577098. doi: 10.3389/fmars.2020.577098

González-Santana, D., González-Dávila, M., Lohan, M. C., Artigue, L., Planquette, H., Sarthou, G., et al. (2021). Variability in iron (II) oxidation kinetics across diverse hydrothermal sites on the northern Mid Atlantic Ridge. *Geochim. Cosmochim. Acta* 297, 143–157. doi: 10.1016/j.gca.2021.01.013

González-Santana, D., Planquette, H., Cheize, M., Whitby, H., Gourain, A., Holmes, T., et al. (2020). Processes driving iron and manganese dispersal from the TAG hydrothermal plume (mid-atlantic ridge): results from a GEOTRACES process study. *Front. Mar. Sci.* 7:568. doi: 10.3389/fmars.2020.00568

Grasshoff, K., Kremling, K., and Ehrhardt, M. (eds) (1999). *Methods of Seawater Analysis*. Hoboken, NJ: Wiley, doi: 10.1002/9783527613984

Haalboom, S., Price, D. M., Mienis, F., van Bleijswijk, J. D. L., de Stigter, H. C., Witte, H. J., et al. (2020). Patterns of (trace) metals and microorganisms in the rainbow hydrothermal vent plume at the Mid-Atlantic Ridge. *Biogeosciences* 17, 2499–2519. doi: 10.5194/bg-17-2499-2020

Hassler, C. S., Sinoir, M., Clementson, L. A., and Butler, E. C. V. (2012). Exploring the link between micronutrients and phytoplankton in the southern ocean during the 2007 Austral Summer. *Front. Microbiol.* 3:1–26. doi: 10.3389/fmicb.2012.00202

Hatta, M., Measures, C. I., Wu, J., Roshan, S., Fitzsimmons, J. N., Sedwick, P., et al. (2015). An overview of dissolved Fe and Mn distributions during the 2010–2011 U.S. GEOTRACES north atlantic cruises: GEOTRACES GA03. *Deep Sea Res. Part II Top. Stud. Oceanogr.* 116, 117–129. doi: 10.1016/j.dsr2.2014.07.005

Hawco, N. J., Ohnemus, D. C., Resing, J. A., Twining, B. S., and Saito, M. A. (2016). A dissolved cobalt plume in the oxygen minimum zone of the eastern tropical South Pacific. *Biogeosciences* 13, 5697–5717. doi: 10.5194/bg-13-5697-2016

Hawkes, J. A., Connelly, D. P., Gledhill, M., and Achterberg, E. P. (2013). The stabilisation and transportation of dissolved iron from high temperature hydrothermal vent systems. *Earth Planet. Sci. Lett.* 375, 280–290. doi: 10.1016/j.epsl.2013.05.047

James, R. H., and Elderfield, H. (1996). Dissolved and particulate trace metals in hydrothermal plumes at the Mid-Atlantic Ridge. *Geophys. Res. Lett.* 23, 3499–3502. doi: 10.1029/96GL01588

Jenkins, W. J., Hatta, M., Fitzsimmons, J. N., Schlitzer, R., Lanning, N. T., Shiller, A., et al. (2020). An intermediate-depth source of hydrothermal 3He and dissolved iron in the North Pacific. *Earth Planet. Sci. Lett.* 539:116223. doi: 10.1016/j.epsl.2020.116223

Jin, X., Chu, Z., Yan, F., and Zeng, Q. (2009). Effects of lanthanum(III) and EDTA on the growth and competition of *Microcystis aeruginosa* and *Scenedesmus quadricauda*. *Limnologica* 39, 86–93. doi: 10.1016/j.limno.2008.03.002

Kim, T., Obata, H., Kondo, Y., Ogawa, H., and Gamo, T. (2015). Distribution and speciation of dissolved zinc in the western North Pacific and its adjacent seas. *Mar. Chem.* 173, 330–341. doi: 10.1016/j.marchem.2014.10.016

Kipp, L. E., Sanial, V., Henderson, P. B., van Beek, P., Reyss, J.-L., Hammond, D. E., et al. (2018). Radium isotopes as tracers of hydrothermal inputs and neutrally buoyant plume dynamics in the deep ocean. *Mar. Chem.* 201, 51–65. doi: 10.1016/j.marchem.2017.06.011

Kleint, C., Bach, W., Diehl, A., Fröhberg, N., Garbe-Schönberg, D., Hartmann, J. F., et al. (2019). Geochemical characterization of highly diverse hydrothermal fluids from volcanic vent systems of the Kermadec intraoceanic arc. *Chem. Geol.* 528:119289. doi: 10.1016/j.chemgeo.2019.119289

Kleint, C., Hawkes, J. A., Sander, S. G., and Koschinsky, A. (2016). Voltammetric investigation of hydrothermal iron speciation. *Front. Mar. Sci.* 3:75. doi: 10.3389/fmars.2016.00075

Lagerström, M. E., Field, M. P., Séguret, M., Fischer, L., Hann, S., and Sherrell, R. M. (2013). Automated on-line flow-injection ICP-MS determination of trace metals (Mn, Fe, Co, Ni, Cu and Zn) in open ocean seawater: application to the

GEOTRACES program. *Mar. Chem.* 155, 71–80. doi: 10.1016/j.marchem.2013.06.001

Lavelle, J. W., Massoth, G. J., Baker, E. T., and de Ronde, C. E. J. (2008). Ocean current and temperature time series at brothers volcano. *J. Geophys. Res.* 113:C09018. doi: 10.1029/2007JC004713

Liu, X., and Millero, F. J. (2002). The solubility of iron in seawater. *Mar. Chem.* 77, 43–54. doi: 10.1016/S0304-4203(01)00074-3

Lough, A. J. M., Homoky, W. B., Connelly, D. P., Nakamura, K., Abyaneh, M. K., Kaulich, B., et al. (2019b). Soluble iron conservation and colloidal iron dynamics in a hydrothermal plume. *Chem. Geol.* 511, 225–237. doi: 10.1016/j.chemgeo.2019.01.001

Lough, A. J. M., Connelly, D. P., Homoky, W. B., Hawkes, J. A., Chavagnac, V., Castillo, A., et al. (2019a). Diffuse hydrothermal venting: a hidden source of iron to the oceans. *Front. Mar. Sci.* 6:329. doi: 10.3389/fmars.2019.00329

Massoth, G. J., De Ronde, C. E. J., Lupton, J. E., Feely, R. A., Baker, E. T., Lebon, G. T., et al. (2003). Chemically rich and diverse submarine hydrothermal plumes of the southern kermadec volcanic arc (New Zealand). *Geol. Soc. London, Spec. Publ.* 219, 119–139. doi: 10.1144/GSL.SP.2003.219.01.06

Millero, F. J., Sotolongo, S., and Izaguirre, M. (1987). The oxidation kinetics of Fe(II) in seawater. *Geochim. Cosmochim. Acta* 51, 793–801. doi: 10.1016/0016-7037(87)90093-7

Moore, W. S. (1976). Sampling 228Ra in the deep ocean. *Deep Sea Res. Oceanogr. Abstr.* 23, 647–651. doi: 10.1016/0011-7471(76)90007-3

Moore, W. S. (2000). Ages of continental shelf waters determined from 223 Ra and 224 Ra. *J. Geophys. Res. Ocean.* 105, 22117–22122. doi: 10.1029/1999JC000289

Moore, W. S., and Arnold, R. (1996). Measurement of 223 Ra and 224 Ra in coastal waters using a delayed coincidence counter. *J. Geophys. Res. Ocean.* 101, 1321–1329. doi: 10.1029/95JC03139

Moore, W. S., and Krest, J. (2004). Distribution of 223Ra and 224Ra in the plumes of the mississippi and atchafalaya rivers and the gulf of mexico. *Mar. Chem.* 86, 105–119. doi: 10.1016/j.marchem.2003.10.001

Morel, F. M. M., Milligan, A. J., and Saito, M. A. (2003). Marine bioinorganic chemistry: the role of trace metals in the oceanic cycles of major nutrients. *Treatise Geochem.* 2014, 113–143. doi: 10.1016/B0-08-043751-6/06108-9

Morris, M., Roemmich, D., and Cornuelle, B. (1996). Observations of variability in the south pacific subtropical gyre. *J. Phys. Oceanogr.* 26, 2359–2380. doi: 10.1175/1520-04851996026<2359:OOVITS<2.0.CO;2

Mottl, M. J., and McConachy, T. F. (1990). Chemical processes in buoyant hydrothermal plumes on the east pacific rise near 21°N. *Geochim. Cosmochim. Acta* 54, 1911–1927. doi: 10.1016/0016-7037(90)90261-I

Neuholz, R., Schnetger, B., Kleint, C., Koschinsky, A., Lettmann, K., Sander, S., et al. (2020b). Near-field hydrothermal plume dynamics at brothers volcano (kermadec arc): a short-lived radium isotope study. *Chem. Geol.* 533:119379. doi: 10.1016/j.chemgeo.2019.119379

Neuholz, R., Kleint, C., Schnetger, B., Koschinsky, A., Laan, P., Middag, R., et al. (2020a). Submarine hydrothermal discharge and fluxes of dissolved fe and mn, and he isotopes at brothers volcano based on radium isotopes. *Minerals* 10, 1–32. doi: 10.3390/min10110969

Noble, A. E., Echegoyen-Sanz, Y., Boyle, E. A., Ohnemus, D. C., Lam, P. J., Kayser, R., et al. (2015). Dynamic variability of dissolved Pb and Pb isotope composition from the U.S. North Atlantic GEOTRACES transect. *Deep Sea Res. Part II Top. Stud. Oceanogr.* 116, 208–225. doi: 10.1016/j.dsr2.2014.11.011

O'Dell, J. W. (1993). *Method 365.1,Determination of Phosphorus By Semi-Automated Colorimetry*. Available online at: https://www.epa.gov/sites/default/files/2015-08/documents/method_365-1_1993.pdf (accessed November 23, 2021).

Resing, J. A., Baker, E. T., Lupton, J. E., Walker, S. L., Butterfield, D. A., Massoth, G. J., et al. (2009). Chemistry of hydrothermal plumes above submarine volcanoes of the Mariana Arc. *Geochem. Geophys. Geosyst.* 10:141. doi: 10.1029/2008GC002141

Resing, J. A., Sedwick, P. N., German, C. R., Jenkins, W. J., Moffett, J. W., Sohst, B. M., et al. (2015). Basin-scale transport of hydrothermal dissolved metals across the South Pacific Ocean. *Nature* 523, 200–203. doi: 10.1038/nature14577

Roemmich, D., and Sutton, P. (1998). The mean and variability of ocean circulation past northern New Zealand: determining the representativeness of hydrographic climatologies. *J. Geophys. Res. Ocean.* 103, 13041–13054. doi: 10.1029/98JC00583

Roshan, S., DeVries, T., Wu, J., John, S., and Weber, T. (2020). Reversible scavenging traps hydrothermal iron in the deep ocean. *Earth Planet. Sci. Lett.* 542:116297. doi: 10.1016/j.epsl.2020.116297

Roshan, S., Wu, J., and Jenkins, W. J. (2016). Long-range transport of hydrothermal dissolved Zn in the tropical South Pacific. *Mar. Chem.* 183, 25–32. doi: 10.1016/j.marchem.2016.05.005

Ruacho, A., Bundy, R. M., Till, C. P., Roshan, S., Wu, J., and Barbeau, K. A. (2020). Organic dissolved copper speciation across the U.S. GEOTRACES equatorial pacific zonal transect GP16. *Mar. Chem.* 225:103841. doi: 10.1016/j.marchem.2020.103841

Rudnicki, M. D., and Elderfield, H. (1993). A chemical model of the buoyant and neutrally buoyant plume above the TAG vent field, 26 degrees N, Mid-Atlantic ridge. *Geochim. Cosmochim. Acta* 57, 2939–2957. doi: 10.1016/0016-7037(93)90285-5

Sander, S. G., and Koschinsky, A. (2011). Metal flux from hydrothermal vents increased by organic complexation. *Nat. Geosci.* 4, 145–150. doi: 10.1038/ngeo1088

Santana-Casiano, J. M., González-Dávila, M., and Millero, F. J. (2006). The role of Fe(II) species on the oxidation of Fe(II) in natural waters in the presence of O2 and H2O2. *Mar. Chem.* 99, 70–82. doi: 10.1016/j.marchem.2005.03.010

Sarradin, P.-M., Waeles, M., Bernagout, S., Le Gall, C., Sarrazin, J., and Riso, R. (2009). Speciation of dissolved copper within an active hydrothermal edifice on the lucky strike vent field (MAR, 37°N). *Sci. Total Environ.* 407, 869–878. doi: 10.1016/j.scitotenv.2008.09.056

Schijf, J., and Byrne, R. H. (2021). Speciation of yttrium and the rare earth elements in seawater: review of a 20-year analytical journey. *Chem. Geol.* 584:120479. doi: 10.1016/j.chemgeo.2021.120479

Schine, C. M. S., Alderkamp, A.-C., van Dijken, G., Gerringa, L. J. A., Sergi, S., Laan, P., et al. (2021). Massive southern ocean phytoplankton bloom fed by iron of possible hydrothermal origin. *Nat. Commun.* 12:1211. doi: 10.1038/s41467-021-21339-5

Schlitzer, R., Anderson, R. F., Dodas, E. M., Lohan, M., Geibert, W., Tagliabue, A., et al. (2018). The GEOTRACES intermediate data product 2017. *Chem. Geol.* 493, 210–223. doi: 10.1016/j.chemgeo.2018.05.040

Schnetger, B., and Lehners, C. (2014). Determination of nitrate plus nitrite in small volume marine water samples using vanadium(III)chloride as a reduction agent. *Mar. Chem.* 160, 91–98. doi: 10.1016/j.marchem.2014.01.010

Statham, P. J., German, C. R., and Connelly, D. P. (2005). Iron (II) distribution and oxidation kinetics in hydrothermal plumes at the Kairei and Edmond vent sites. *Indian Ocean. Earth Planet. Sci. Lett.* 236, 588–596. doi: 10.1016/j.epsl.2005.03.008

Stichel, T., Pahnke, K., Duggan, B., Goldstein, S. L., Hartman, A. E., Paffrath, R., et al. (2018). TAG plume: revisiting the hydrothermal neodymium contribution to seawater. *Front. Mar. Sci.* 5:96. doi: 10.3389/fmars.2018.00096

Stüben, D., Stoffers, P., Cheminée, J.-L., Hartmann, M., McMurtry, G. M., Richnow, H.-H., et al. (1992). Manganese, methane, iron, zinc, and nickel anomalies in hydrothermal plumes from teahitia and macdonald volcanoes. *Geochim. Cosmochim. Acta* 56, 3693–3704. doi: 10.1016/0016-7037(92)90162-C

Sültenfuß, J., Roether, W., and Rhein, M. (2009). The Bremen mass spectrometric facility for the measurement of helium isotopes, neon, and tritium in water†. *Isotopes Environ. Health Stud.* 45, 83–95. doi: 10.1080/10256010902871929

Sunda, W. G. (1988). Trace metal interactions with marine phytoplankton. *Biol. Oceanogr.* 6, 411–442.

Sutton, P., Chiswell, S., Gorman, R., Kennan, S., and Rickard, G. (2012). *Physical Marine Environment of the Kermadec Islands Region.* Wellington: Department of Conservation.

Tagliabue, A. (2014). More to hydrothermal iron input than meets the eye: fig. 1. *Proc. Natl. Acad. Sci. U.S.A.* 111, 16641–16642. doi: 10.1073/pnas.1419829111

Toner, B. M., Fakra, S. C., Manganini, S. J., Santelli, C. M., Marcus, M. A., Moffett, J. W., et al. (2009). Preservation of iron(II) by carbon-rich matrices in a hydrothermal plume. *Nat. Geosci.* 2, 197–201. doi: 10.1038/ngeo433

van den Berg, C. M. G. (2000). *Determination of Organic Complexation," in Chemical Processes in Marine Environments*. Berlin, Heidelberg: Springer Berlin Heidelberg, 175–187. doi: 10.1007/978-3-662-04207-6_9

Visbeck, M. (2002). Deep velocity profiling using lowered acoustic doppler current profilers: bottom track and inverse solutions*. *J. Atmos. Ocean. Technol.* 19, 794–807. doi: 10.1175/1520-04262002019<0794:DVPULA<2.0.CO;2

Walker, S. L., de Ronde, C. E. J., and Baker, E. T. (2018). "Two decades of monitoring hydrothermal plumes at the brothers submarine arc volcano, Kermadec arc, New Zealand," in *Proceedings of the AGU Fall Meeting 2018*, San Francisco, CA.

Wheat, C. G., Feely, R. A., and Mottl, M. J. (1996). Phosphate removal by oceanic hydrothermal processes: an update of the phosphorus budget in the oceans. *Geochim. Cosmochim. Acta* 60, 3593–3608.

Whitfield, M. (2001). Interactions between phytoplankton and trace metals in the ocean. *Adv. Mar. Biol.* 41, 1–128. doi: 10.1016/S0065-2881(01)41002-9

Wright, I. C. (2001). In situ modification of modern submarine hyaloclastic/pyroclastic deposits by oceanic currents: an example from the southern kermadec arc (SW pacific). *Mar. Geol.* 172, 287–307. doi: 10.1016/S0025-3227(00)00131-6

Yücel, M., Gartman, A., Chan, C. S., and Luther, G. W. (2011). Hydrothermal vents as a kinetically stable source of iron-sulphide-bearing nanoparticles to the ocean. *Nat. Geosci.* 4, 367–371. doi: 10.1038/ngeo1148

Conflict of Interest: The authors declare that the research was conducted in the absence of any commercial or financial relationships that could be construed as a potential conflict of interest.

Publisher's Note: All claims expressed in this article are solely those of the authors and do not necessarily represent those of their affiliated organizations, or those of the publisher, the editors and the reviewers. Any product that may be evaluated in this article, or claim that may be made by its manufacturer, is not guaranteed or endorsed by the publisher.